Chapter 3
Figures of Merit of Modern Piezo-Active Ceramics and Composites

In the past decades, various figures of merit have been introduced to characterise the effectiveness of modern functional materials in the context of their piezoelectric and/or pyroelectric properties [1–5]. Knowledge of the figures of merit is important because of the links to various forms of energy and its transformation for exploitation of the functional materials as active elements in electronic circuits and devices. In the case of piezoelectric transducers, a number of figure of merits have been put forward to take into account the oscillation mode, the nature of the external loading, and the output conditions [see (1.30)–(1.32)]. For instance, piezoelectric transducers, transmit-receive systems and pulse-echo systems for broad-band airborne ultrasound applications can be described in terms of the figure of merit [7] that is regarded as a ratio of the electric power measured at the receiver output to the electric input power applied to the transmitter. Such a parameter is of value when dealing with a composite transducer that comprises of components with contrasting electromechanical properties. As follows from various literature data, various figures of merit suitable for piezoelectric materials are concerned with their piezoelectric coefficients, ECFs, specific acoustic impedance, quality factor, etc. In hydroacoustic applications, the relevant figure of merit strongly depends on the hydrostatic piezoelectric response of the active element [1, 7, 8]. As noted by Sessler and Hillenbrand [3], the choice of the figure of merit depends on the application for which the piezoelectric materials being used.

In this chapter we discuss examples of the figures of merit of various piezoelectric materials, that may be suitable for energy-harvesting applications, and links between the figures of merit and piezoelectric performance of these materials.

3.1 Poled Ferroelectric Ceramics

Values of squared figures of merit from (1.30)–(1.32) can vary in relatively wide ranges (Table 3.1). We arrange the perovskite-type poled FCs on $(Q_{33})^2$ that is concerned with the longitudinal piezoelectric effect. The largest $(Q_{33})^2$ values are

C.R. Bowen et al., *Modern Piezoelectric Energy-Harvesting Materials*,
Springer Series in Materials Science 238, DOI 10.1007/978-3-319-29143-7_3

achieved in the soft PCR-type FCs. The large $(Q_{33})^2$ value related to PZ 27 is accounted for by the relatively small dielectric permittivity $\varepsilon_{33}^{\sigma}$ in comparison to that of PCR-73 or PCR-7M. The relatively small $(Q_{33})^2$ value is achieved in the $PbTiO_3$-type FCs We remind the reader that the values of $(Q_{3j})^2$ in Table 3.1 are related to a low-frequency range [2–4] which is far from any resonance frequency of the piezoelectric element.

Data from Table 3.1 suggest that the inequality

$$(Q_{33})^2 \gg (Q_h)^2 \tag{3.1}$$

Table 3.1 Squared figures of merit $(Q_{3j})^2$ and $(Q_h)^2$ (in 10^{-12} Pa^{-1}) of perovskite-type FCs[a] at room temperature

FC	$(Q_{33})^2$	$(Q_{31})^2$	$(Q_h)^2$
PCR-73, hp[b]	13.9	2.72	0.188
PCR-7M, hp	13.1	2.77	0.0203
PCR-7, hp	12.0	2.53	0.0807
PZ 27	11.2	1.93	0.322
PZT-5	9.25	1.92	0.0724
PCR-1, hp	8.41	1.57	0.156
$Pb(Zr_{0.52}Ti_{0.48})O_3$	7.70	1.35	0.201
PZT-4	7.48	1.36	0.163
$(Pb_{0.94}Sr_{0.06})(Ti_{0.47}Zr_{0.53})O_3$	7.26	1.31	0.161
ZTS-19	7.10	1.20	0.228
PCR-8, ct	6.81	1.36	0.0782
PCR-8, hp	6.79	1.36	0.0726
PZT-7A	6.03	0.959	0.248
$Pb(Zr_{0.54}Ti_{0.46})O_3$	5.80	0.910	0.251
PCR-21, hp	5.23	0.994	0.0857
PZT-5H	4.50	0.743	0.158
$BaTiO_3$ (II)	2.40	0.404	0.0768
$BaTiO_3$ (I)	2.17	0.371	0.0648
PZ 34	2.01	0.00886	1.51
PCR-63, hp	1.89	0.348	0.0386
Modified $PbTiO_3$ (II)	1.87	0.0275	1.07
Modified $PbTiO_3$ (I)	1.66	0.0124	1.14
$(Pb_{0.855}Nd_{0.11})(Ti_{0.94}Mn_{0.02}In_{0.04})O_3$	1.53	0.0187	0.927
$(Pb_{0.9625}La_{0.025})(Ti_{0.99}Mn_{0.01})O_3$	1.50	0.0116	1.02
$(Pb_{0.85}Nd_{0.10})(Ti_{0.99}Mn_{0.01})O_3$	1.45	0.0132	0.947

[a]Full sets of electromechanical constants of the FCs are given in Table 1.2

[b]FC samples of the PCR type have been manufactured using either the conventional technology (ct) or hot pressing (hp). PCR is the abbreviation for the group "piezoelectric ceramics from Rostov-on-Don" (Russia) [7, 9, 10]

is not valid in the $PbTiO_3$-type FCs due to their large piezoelectric anisotropy The large piezoelectric anisotropy promotes a validity of the condition

$$(Q_{33})^2 \gg (Q_{31})^2 \tag{3.2}$$

irrespective of dielectric properties of the $PbTiO_3$-type FCs. It is noted that the poled FC is characterised by ∞mm symmetry [11, 12], and therefore, the equality $(Q_{31})^2 = (Q_{32})^2$ holds in the case of the poling axis OX_3.

Our numerous data show that the values of $(Q_{3j})^2$ and $(Q_h)^2$ from Table 3.1 remain relatively small in comparison to those achieved in various composites based on either FCs or relaxor-ferroelectric domain-engineered SCs [7, 10]. In Sects. 3.2–3.5 we discuss examples of large $(Q_{3j})^2$ and $(Q_h)^2$ for a number of connectivity patterns.

3.2 2–2 Composites

3.2.1 Ceramic/Polymer Composites

The 2–2 composite [7, 8, 10] is characterised by a continuous distribution of each component along two axes of a rectangular co-ordinate system ($X_1X_2X_3$). Such a composite can be regarded as a laminar structure wherein the components (layers) are alternating along the third axis of ($X_1X_2X_3$). The relative simplicity of the laminar structure and the possibility of varying the volume fractions of the components in a wide range allow the manufacture and design of 2–2 composites with tailored (e.g., extreme) values of their effective parameters. Methods to manufacture the 2–2 FC/polymer composites are discussed in review papers (see, for instance, [13–15]).

The 2–2 FC/polymer composites are usually manufactured in two modifications: with a series connection of adjacent layers (Fig. 3.1a) and with a parallel connection of adjacent layers (Fig. 3.1b). In the series-connected composite, the C1 and C2 layers are alternating in the OX_3 direction (Fig. 3.1a) and interfaces are perpendicular to OX_3, and this co-ordinate axis is the poling axis. In the parallel-connected composite, the poling axis OX_3 is parallel to the interfaces that separate the C1 and C2 layers (Fig. 3.1b). It is obvious that these two modifications are characterised by different electromechanical properties [7, 10] and anisotropy because of different orientations of the interfaces with respect to the poling axis OX_3. In the series-connected composite, the piezoelectric coefficients d^*_{3j} concerned with the poling axis obey the condition $d^*_{31} = d^*_{32} \neq d^*_{33}$. The piezoelectric coefficients d^*_{3j} of the parallel-connected composite satisfy the condition $d^*_{31} \neq d^*_{32} \neq d^*_{33}$ [7]. Based on these conditions, we state that the hydrostatic piezoelectric coefficient of the FC/polymer composite is represented in the general form as

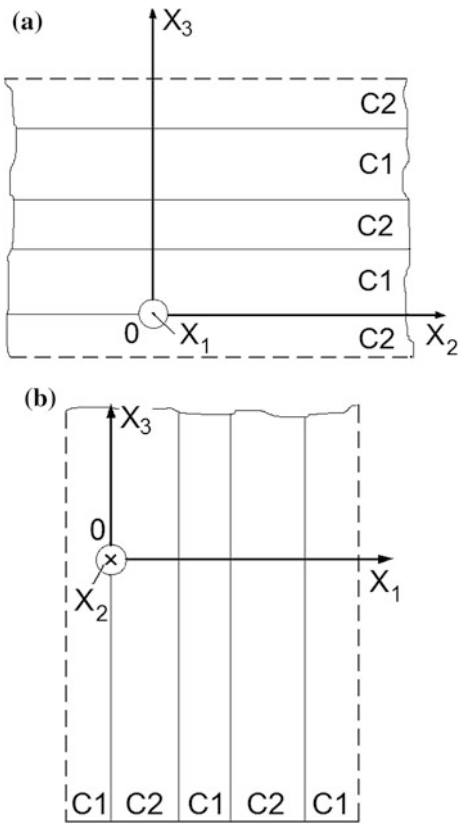

Fig. 3.1 Schematic of the 2–2 series-connected (**a**) and parallel-connected (**b**) composites with components denoted as C1 and C2. ($X_1X_2X_3$) is the rectangular co-ordinate system, and OX_3 is the poling direction (reprinted from monograph by Topolov et al. [10], with permission from Springer)

$$d_h^* = d_{31}^* + d_{32}^* + d_{33}^*. \tag{3.3}$$

Equation (3.3) is written on assumption that electrodes applied to the composite sample are perpendicular to the poling axis OX_3.

The effective electromechanical properties of the 2–2 composite are determined within the framework of the matrix approach [7, 10]. This approach is suitable for components with arbitrary symmetry of their properties at arbitrary volume fractions of the C1 and C2 components (Fig. 3.1). We assume that m is the volume fraction of the C1 component, and $1 - m$ is the volume fraction of the C2 component. The matrix of the effective electromechanical properties of the composite in the co-ordinate system ($X_1X_2X_3$) is written in the general form as

$$\|C^*\| = \begin{pmatrix} \|s^{*E}\| & \|d^*\|^t \\ \|d^*\| & \|\varepsilon^{*\sigma}\| \end{pmatrix}. \tag{3.4}$$

In (3.4),$\| s^{*E} \|$ is the matrix of elastic compliances at electric field E = const (6 × 6 matrix), $\| d^* \|$ is the matrix of piezoelectric coefficients (3 × 6 matrix), $\| \varepsilon^{*\sigma} \|$ is

the matrix of dielectric permittivities at mechanical stress σ = const (3 × 3 matrix), and superscript 't' denotes the transposed matrix. The $\| C^* \|$ matrix from (3.4) is determined by averaging the electromechanical properties of the components on m and written as follows:

$$||C^*|| = [\left|\left|C^{(1)}\right|\right| \cdot ||M||m + \left|\left|C^{(2)}\right|\right|(1-m)] \cdot [||M||m + ||I||(1-m)]^{-1}. \quad (3.5)$$

In (3.5), $\| C^{(1)} \|$ and $\| C^{(2)} \|$ are matrices of the electromechanical properties of the FC (or C1) and polymer (or C2), respectively, $\| M \|$ is concerned with the electric and mechanical boundary conditions [7, 10] at interfaces (Fig. 3.1), and $\| I \|$ is the identity 9 × 9 matrix.

For example, in the case of the parallel-connected composite (Fig. 3.1b) with interfaces x_1 = const, the boundary conditions imply a continuity of components of mechanical stress $\sigma_{11} = \sigma_1$, $\sigma_{12} = \sigma_6$ and $\sigma_{13} = \sigma_5$, strain $\xi_{22} = \xi_2$, $\xi_{23} = \xi_4/2$ and $\xi_{33} = \xi_3$, electric displacement D_1, and electric field E_2 and E_3. The $\| M \|$ matrix from (3.5) is written for x_1 = const as $\| M \| = \| m_1 \|^{-1} \| m_2 \|$, where

$$||m_n|| = \begin{pmatrix} 1 & 0 & 0 & 0 & 0 & 0 & 0 & 0 & 0 \\ s_{12}^{(n),E} & s_{22}^{(n),E} & s_{23}^{(n),E} & s_{24}^{(n),E} & s_{25}^{(n),E} & s_{26}^{(n),E} & d_{12}^{(n)} & d_{22}^{(n)} & d_{32}^{(n)} \\ s_{13}^{(n),E} & s_{23}^{(n),E} & s_{33}^{(n),E} & s_{34}^{(n),E} & s_{35}^{(n),E} & s_{36}^{(n),E} & d_{13}^{(n)} & d_{23}^{(n)} & d_{33}^{(n)} \\ s_{14}^{(n),E} & s_{24}^{(n),E} & s_{34}^{(n),E} & s_{44}^{(n),E} & s_{45}^{(n),E} & s_{46}^{(n),E} & d_{14}^{(n)} & d_{24}^{(n)} & d_{34}^{(n)} \\ 0 & 0 & 0 & 0 & 1 & 0 & 0 & 0 & 0 \\ 0 & 0 & 0 & 0 & 0 & 1 & 0 & 0 & 0 \\ d_{11}^{(n)} & d_{12}^{(n)} & d_{13}^{(n)} & d_{14}^{(n)} & d_{15}^{(n)} & d_{16}^{(n)} & \varepsilon_{11}^{(n),\sigma} & \varepsilon_{12}^{(n),\sigma} & \varepsilon_{13}^{(n),\sigma} \\ 0 & 0 & 0 & 0 & 0 & 0 & 0 & 1 & 0 \\ 0 & 0 & 0 & 0 & 0 & 0 & 0 & 0 & 1 \end{pmatrix}$$

is represented using electromechanical constants of C1 (at n = 1) or C2 (at n = 2). We add that $\| m_n \|$ can be written taking into account the specific symmetry of each component. It should be noted that the effective electromechanical properties in (3.5) are determined in the longwave approximation [7], i.e., the wavelength of the external acoustic field is much greater than the width of each layer of the composite sample (Fig. 3.1).

Based on (3.4) and (3.5) and conventional formulae for the piezoelectric medium [11, 12], we obtain the effective parameters of the 2–2 composite at volume fractions of FC $0 < m < 1$. By analogy with (1.30)–(1.32), we represent squared figures of merit of the composite as

$$\left(Q_{3j}^*\right)^2 = d_{3j}^* g_{3j}^* \text{ and } \left(Q_h^*\right)^2 = d_h^* g_h^*, \quad (3.6)$$

where $j = 1, 2$ and 3, and

$$g_h^* = g_{31}^* + g_{32}^* + g_{33}^* \tag{3.7}$$

is the hydrostatic piezoelectric coefficient that characterises the sensitivity of the composite under hydrostatic loading.

Table 3.2 shows the volume-fraction dependence of the squared figures of merit $\left(Q_{3j}^*\right)^2$ of the 2–2 composite with a parallel connection of layers. This composite is based on the typical PZT-type FC. The parallel connection of the layers (Fig. 3.1b) that are continuous along OX_2 and OX_3 enables us to achieve large values of d_{33}^* and $\left|d_{32}^*\right|$ at relatively small volume fractions of FC m. A slow monotonic increase of $\varepsilon_{33}^{*\sigma}(m)$ and a rapid monotonic increase of $\left|d_{3j}^*(m)\right|$ at $m << 1$ lead to $\max\left|g_{3j}^*(m)\right|$ and $\max\left[Q_{3j}^*(m)\right]^2$ [7]. It should be added that $\left[Q_{33}^*(m)\right]^2$ undergoes greater changes at $0 < m < 1$ in comparison to $\left[Q_{31}^*(m)\right]^2$ and $\left[Q_{32}^*(m)\right]^2$ (see Table 3.2). This is due to the more pronounced piezoelectric activity of the composite along OX_3 where the considerable longitudinal piezoelectric effect of FC plays a dominating role.

Another example of the volume-fraction behaviour of $\left[Q_{3j}^*(m)\right]^2$ is given in Table 3.3. The performance of the 2–2 composite based on the highly anisotropic

Table 3.2 Volume-fraction dependences of the piezoelectric coefficients d_{3j}^* (in pC/N), g_{3j}^* (in mV m/N) and squared figures of merit $\left(Q_{3j}^*\right)^2$ (in 10^{-12} Pa^{-1}), which have been calculated for the 2–2 PZT-5 FC/araldite parallel-connected composite

m	d_{31}^*	d_{32}^*	d_{33}^*	g_{31}^*	g_{32}^*	g_{33}^*	$\left(Q_{31}^*\right)^2$	$\left(Q_{32}^*\right)^2$	$\left(Q_{33}^*\right)^2$
0	0	0	0	0	0	0	0	0	0
0.05	–43.7	–61.2	136	–79.4	–111	247	3.47	6.79	33.6
0.1	–67.0	–92.4	205	–55.7	–76.8	170	3.73	7.10	34.9
0.2	–93.1	–124	273	–35.2	–46.9	103	3.28	5.82	28.1
0.3	–109	–140	307	–26.3	–33.7	74.0	2.87	4.72	22.7
0.4	–121	–149	328	–21.3	–26.2	57.6	2.58	3.90	18.9
0.5	–131	–156	342	–18.1	–21.5	47.2	2.37	3.35	16.1
0.6	–140	–160	352	–15.9	–18.2	40.0	2.23	2.91	14.1
0.7	–148	–163	359	–14.3	–15.8	34.6	2.12	2.58	12.4
0.8	–155	–167	365	–13.1	–13.9	30.6	2.03	2.32	11.2
0.9	–163	–169	369	–12.1	–12.5	27.3	1.97	2.11	10.1
1	–170	–170	373	–11.3	–11.3	24.8	1.92	1.92	9.25

Note Extreme points of $g_{3j}^*(m)$ are $\min g_{31}^* = g_{31}^*(0.016) = -102$ mV m/N, $\min g_{32}^* = g_{32}^*(0.016) = -143$ mV m/N and $\max g_{33}^* = g_{33}^*(0.015) = 320$ mV m/N

Table 3.3 Volume-fraction dependences of the piezoelectric coefficients d_{3j}^{*} (in pC/N), g_{3j}^{*} (in mV m/N) and squared figures of merit $\left(Q_{3j}^{*}\right)^{2}$ (in 10^{-12} Pa^{-1}), which have been calculated for the 2–2 modified $PbTiO_3$ (I) FC/araldite parallel-connected composite

m	d_{31}^{*}	d_{32}^{*}	d_{33}^{*}	g_{31}^{*}	g_{32}^{*}	g_{33}^{*}	$\left(Q_{31}^{*}\right)^{2}$	$\left(Q_{32}^{*}\right)^{2}$	$\left(Q_{33}^{*}\right)^{2}$
0	0	0	0	0	0	0	0	0	0
0.05	–12.3	–5.22	28.8	–116	–49.1	270	1.43	0.256	7.78
0.1	–15.9	–5.39	37.2	–88.0	–29.8	205	1.40	0.161	7.63
0.2	–17.6	–5.11	43.8	–52.8	–15.3	131	0.929	0.0781	5.74
0.3	–17.1	–4.89	46.5	–35.1	–10.0	95.4	0.600	0.0489	4.44
0.4	–15.8	–4.75	48.0	–24.7	–7.40	74.9	0.390	0.0329	3.60
0.5	–14.2	–4.64	49.0	–17.8	–5.84	61.6	0.253	0.0271	3.02
0.6	–12.4	–4.57	49.6	–13.1	–4.81	52.3	0.159	0.0220	2.59
0.7	–10.5	–4.51	50.1	–9.50	–4.09	45.4	0.0998	0.0184	2.27
0.8	–8.50	–4.47	50.5	–6.76	–3.55	40.1	0.0575	0.0159	2.03
0.9	–6.47	–4.43	50.8	–4.58	–3.14	35.9	0.0296	0.0139	1.82
1	–4.40	–4.40	51.0	–2.81	–2.81	32.6	0.0124	0.0124	1.66

Note Extreme points of $d_{3j}^{*}(m)$ and $g_{3j}^{*}(m)$ are listed as follows: min $d_{31}^{*} = d_{31}^{*}(0.207) = -17.6$ pC/N, min $d_{32}^{*} = d_{32}^{*}(0.085) = -5.41$ pC/N, min $g_{31}^{*} = g_{31}^{*}(0.034) = -121$ mV m/N, min $g_{32}^{*} = g_{32}^{*}(0.021) = -62.8$ mV m/N, and max $g_{33}^{*} = g_{33}^{*}(0.031) = 285$ mV m/N

$PbTiO_3$-type FC suggests that $\max\left[Q_{3j}^{*}(m)\right]^{2}$ are smaller than those in the 2–2 composite based on PZT-5 (see Table 3.2). The squared figure of merit $\left[Q_{33}^{*}(m)\right]^{2}$ of the 2–2 composite based on the $PbTiO_3$-type FC undergoes changes in a narrower range. This behaviour is a result of the lower piezoelectric activity of the $PbTiO_3$-type FC in comparison to the piezoelectric activity of the PZT-type FC. For instance, the piezoelectric coefficient $d_{33}^{(1)}$ of the modified $PbTiO_3$ (I) FC is approximately 7.3 times less than $d_{33}^{(1)}$ of the PZT-5 FC (see Table 3.2). The difference between values of $d_{31}^{(1)}$ of the aforementioned FCs is more pronounced. Thus, the 2–2 composite based on the PZT-type FC becomes preferable in the context of its squared figures of merit $\left[Q_{3j}^{*}(m)\right]^{2} \gg \left(Q_{3j}^{(1)}\right)^{2}$.

We add that the series connection of the composite layers (Fig. 3.1a) lead to a low piezoelectric activity and small values of $\left[Q^{*}_{3j}(m)\right]^2$ due to interfaces that weaken the longitudinal piezoelectric effect despite the large $d^{(1)}_{33}$ value of the FC.

In general, the 2–2 FC/composite with a parallel connection of layers (Fig. 3.1b) is of value as a piezoelectric anisotropic material with squared figures of merit $\left[Q^{*}_{3j}(m)\right]^2$ that vary in wide ranges, and maxima of these parameters can be achieved at volume fractions of FC $m \approx 0.1$.

3.2.2 Single Crystal/Polymer Composites

Domain-engineered perovskite-type relaxor-ferroelectric PMN–*x*PT SCs with compositions near the morphotropic phase boundary [15–18] exhibit outstanding electromechanical properties that are of value for various piezotechnical applications. The high piezoelectric performance of the PMN–*x*PT SC/polymer composites [7, 10, 19–21] is important for such applications as active elements of energy harvesters, sensors, actuators, transducers, hydrophones, and acoustic antennae. A potential mechanism for improving the figures of merit is related to optimising the orientation of the main crystallographic axes [10] in the SC component.

The first example to be discussed is concerned with the parallel-connected 2–2 composite based on PMN–0.28PT SC. This composition is located close to the morphotropic phase boundary and can be regarded as a good candidate for the SC component in modern piezo-active composites. The PMN–0.28PT SC has been the first perovskite-type relaxor-ferroelectric SC, for which self-consistent and complete sets of electromechanical constants (Table 3.4) have been measured along three poling directions, namely, along [111], [001] and [011] in the perovskite unit cell [22]. As follows from experimental room-temperature data [22], the single-domain PMN–0.28PT SC is characterised by 3*m* symmetry with a spontaneous polarisation vector $\boldsymbol{P}_s^{(1)} \parallel [111]$. The domain-engineered PMN–0.28PT SC poled along [001] exhibits 4*mm* symmetry and has an average spontaneous polarisation vector $\boldsymbol{P}_s^{(1)} \parallel [001]$. The domain-engineered PMN–0.28PT SC poled along [011] leads to the domain-engineered state with *mm*2 symmetry and an average spontaneous polarisation vector $\boldsymbol{P}_s^{(1)} \parallel [011]$. Liu et al. [22] underlined that the complete sets of electromechanical constants for the three crystallographic orientations (or poling directions) were determined from the same PMN–0.28PT crystal wafer, so that the composition and properties are uniform. It is seen from Table 3.4 that different poling directions lead to the different piezoelectric activity and anisotropy of the properties in PMN–0.28PT SCs. In this connection it is important to show advantages of the specific crystallographic orientation of the main crystallographic axes of the SC component at forming the piezoelectric response and figures of merit of the 2–2 SC/polymer composite.

Table 3.4 Elastic compliances $s_{ab}^{(n),E}$ (in 10^{-12} Pa^{-1}), piezoelectric coefficients $d_{ij}^{(n)}$ (in pC/N) and relative dielectric permittivity $\varepsilon_{pp}^{(n),\sigma}/\varepsilon 0$ of the poled PMN–0.28PT SC at room temperature [22]. Data on the [001]- and [011]-poled SCs are given with respect to the main crystallographic axes

Electromechanical constant	Single-domain [111]-poled SC, $3m$ symmetry	Polydomain [001]-poled SC, $4mm$ symmetry	Polydomain [011]-poled SC, $mm2$ symmetry
$s_{11}^{(n),E}$	8.78	44.57	13.40
$s_{12}^{(n),E}$	–4.90	–28.91	–21.18
$s_{13}^{(n),E}$	–0.93	–13.91	12.67
$s_{14}^{(n),E}$	16.87	0	0
$s_{22}^{(n),E}$	8.78	44.57	54.36
$s_{23}^{(n),E}$	–0.93	–13.91	–33.59
$s_{33}^{(n),E}$	6.32	34.38	28.02
$s_{44}^{(n),E}$	138.69	15.22	15.22
$s_{55}^{(n),E}$	138.69	15.22	147.06
$s_{66}^{(n),E}$	27.4	16.34	22.47
$d_{15}^{(n)}$	2382	122	2162
$d_{22}^{(n)}$	–312	0	0
$d_{24}^{(n)}$	2382	122	160
$d_{31}^{(n)}$	–43	–569	447
$d_{32}^{(n)}$	–43	–569	–1150
$d_{33}^{(n)}$	97	1182	860
$\varepsilon_{11}^{(n),\sigma}/\varepsilon_0$	4983	1672	4235
$\varepsilon_{22}^{(n),\sigma}/\varepsilon_0$	4983	1672	1081
$\varepsilon_{33}^{(n),\sigma}/\varepsilon_0$	593	5479	3873

Now we consider the 2–2 parallel-connected SC/polymer composite wherein a regular distribution of layers on the OX_1 direction is observed (Fig. 3.2). The SC and polymer layers are distributed continuously on the OX_2 and OX_3 directions. An orientation of the spontaneous polarisation vector $\boldsymbol{P}_s^{(1)}$ in each single-domain SC layer is characterised by the Euler angles φ, ψ and θ (Fig. 3.2, inset 1). The x, y and z axes are the main crystallographic axes in polydomain states (Fig. 3.2, insets 2 and 3). Interconnections between the spontaneous polarisation vectors $\boldsymbol{P}_{s,k}$ of several domain types and the spontaneous polarisation vector $\boldsymbol{P}_s^{(1)}$ of the polydomain SC layer are shown in insets 2 and 3 of Fig. 3.2. Hereby we note that $\boldsymbol{P}_s^{(1)} \parallel$ z in both cases. The polymer layers are ferroelectric with a remanent polarisation vector $\boldsymbol{P}_r^{(2)} \uparrow\downarrow OX_3$ (Fig. 3.2, inset 4). At this antiparallel orientation of $\boldsymbol{P}_r^{(2)}$ and OX_3, signs of the piezoelectric coefficients $d_{ij}^{(2)}$ of polyvinylidene fluoride (PVDF,

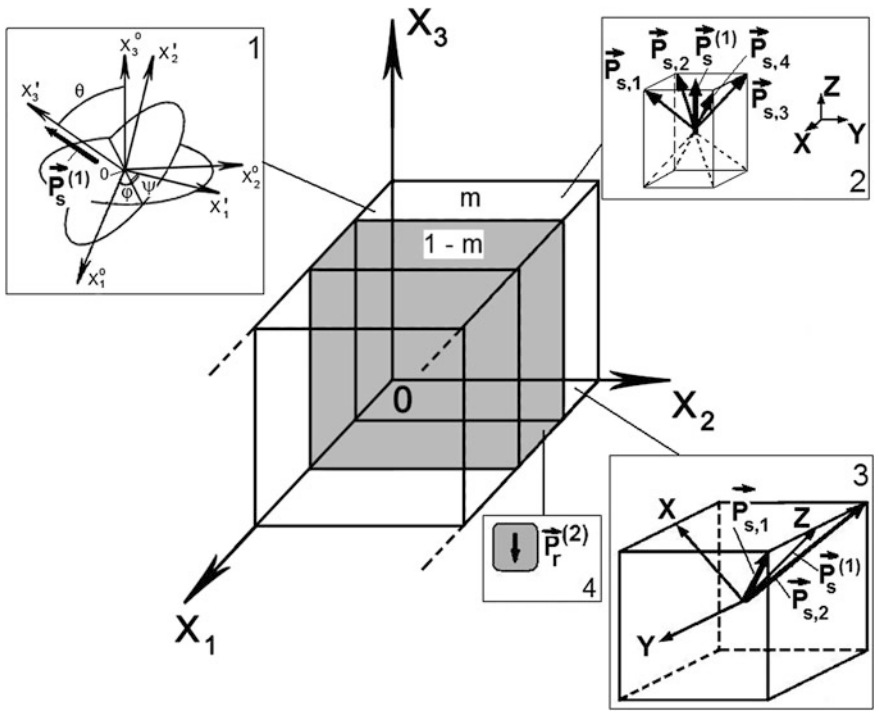

Fig. 3.2 Schematic of the 2–2 SC/polymer composite with parallel-connected layers. ($X_1X_2X_3$) is a rectangular co-ordinate system, m and $1 - m$ are volume fractions of SC and polymer, respectively, $\boldsymbol{P}_s^{(1)}$ and $\boldsymbol{P}_r^{(2)}$ are the spontaneous polarisation vector of SC and the remanent polarisation vector of polymer, respectively. In *inset 1* φ, ψ and θ are Euler angles that characterise a rotation of the main crystallographic axes $\left(X_1^oX_2^oX_3^o\right) \rightarrow \left(X_1'X_2'X_3'\right)$ and the $\boldsymbol{P}_s^{(1)}$ vector in each single-domain [111]-poled SC layer. *Inset 2* comprises domain orientations in the [001]-poled SC with the effective spontaneous polarisation vector $\boldsymbol{P}_s^{(1)}$, *inset 3* comprises domain orientations in the [011]-poled SC with the effective spontaneous polarisation vector $\boldsymbol{P}_s^{(1)}$. $\boldsymbol{P}_{s,1}$, $\boldsymbol{P}_{s,2}$, $\boldsymbol{P}_{s,3}$, and $\boldsymbol{P}_{s,4}$ are spontaneous polarisation vectors of several domain types. x, y and z are main crystallographic axes of the polydomain SCs. The remanent polarisation vector of polymer $\boldsymbol{P}_r^{(2)} \uparrow\downarrow OX_3$ is shown in *inset 4* (reprinted from paper by Topolov et al. [27], with permission from Taylor and Francis)

Table 3.5) coincide [23] with $\mathrm{sgn}d_{ij}$ of conventional PZT-type FCs (see, for instance, Table 1.2). Manufacturing of the studied 2–2 composite with various orientations of the $\boldsymbol{P}_s^{(1)}$ and $\boldsymbol{P}_r^{(2)}$ vectors can be achieved by poling the ferroelectric components separately. As follows from literature data, the coercive fields $E_c^{(n)}$ of the single-domain PMN–xPT SCs [24, 25] and PVDF [26] obey the condition $E_c^{(1)} \ll E_c^{(2)}$ which favours the potential to individually pole the relaxor-ferroelectric SC and the ferroelectric polymer components.

Table 3.5 Elastic compliances $s_{ab}^{(n),E}$ (in 10^{-12} Pa^{-1}), piezoelectric coefficients $d_{ij}^{(n)}$ (in pC/N) and relative dielectric permittivity $\varepsilon_{pp}^{(n),\sigma}/\varepsilon_0$ of poled PVDF with $\boldsymbol{P}_r^{(2)} \uparrow\downarrow OX_3$ (∞mm symmetry) at room temperature [23]

Electromechanical constant	PVDF
$s_{11}^{(n),E}$	333
$s_{12}^{(n),E}$	–148
$s_{13}^{(n),E}$	–87.5
$s_{33}^{(n),E}$	299
$s_{44}^{(n),E}$	$1.90 \cdot 10^4$
$s_{66}^{(n),E}$	943
$d_{15}^{(n)}$	38
$d_{31}^{(n)}$	–10.42
$d_{33}^{(n)}$	33.64
$\varepsilon_{11}^{(n),\sigma}/\varepsilon_0$	7.513
$\varepsilon_{22}^{(n),\sigma}/\varepsilon_0$	7.513
$\varepsilon_{33}^{(n),\sigma}/\varepsilon_0$	8.431

Hereafter we distinguish the SC/polymer composites [27] with the following SC layers:

(i) Composite-1 with the single-domain layers (see Fig. 3.2, inset 1),
(ii) Composite-2 with the polydomain [001]-poled layers (see Fig. 3.2, inset 2) and
(iii) Composite-3 with the polydomain [011]-poled layers (see Fig. 3.2, inset 3).

The single-domain state in the SC layers of Composite-1 is stabilised by a bias field applied along the $\boldsymbol{P}_s^{(1)}$ vector. Rotations of the co-ordinate axes $\left(X_1^o X_2^o X_3^o\right) \rightarrow \left(X_1' X_2' X_3'\right)$ (Fig. 3.2, inset 1) mean the rotations of the spontaneous polarisation vector $\boldsymbol{P}_s^{(1)}$ and the crystallographic axes of the single-domain SC layer. The co-ordinate axes OX_k^o and OX_k' (k = 1, 2 or 3) coincide at $\varphi = \psi = \theta = 0°$. In Composite-2 and Composite-3, where the SC layer comprises different domain types, we consider the rotation of the main crystallographic axes x, y and z of the SC layer around one of the co-ordinate axes, namely, $OX_1 \parallel$ x, $OX_2 \parallel$ y or $OX_3 \parallel$ z (Fig. 3.3). It is assumed that at these rotations, the spontaneous polarisation vectors of individual domains $\boldsymbol{P}_{s,1}$, $\boldsymbol{P}_{s,2}$ etc. in the SC layer are situated either over or in the $(X_1 OX_2)$ plane (see Fig. 3.2). In this case the rotation angles are varied in the following ranges:

(i) for Composite-1, $0° \le \varphi \le 120°$ (due to $3m$ symmetry of the single-domain SC, the upper limit is taken at 120° instead of 360°), $0° \le \psi \le 360°$ and $0° \le \theta \le 180°$ (Fig. 3.2, inset 1),
(ii) for Composite-2, $-45° \le \delta_x \le 45°$ and $-45° \le \delta_y \le 45°$ (Fig. 3.3a), and
(iii) for Composite-3, $-\arcsin\left(1/\sqrt{3}\right) \le \alpha \le \arcsin\left(1/\sqrt{3}\right)$, $-45° \le \beta \le 45°$ and $0° \le \gamma \le 360°$ (see Fig. 3.3b and inset 3 in Fig. 3.2).

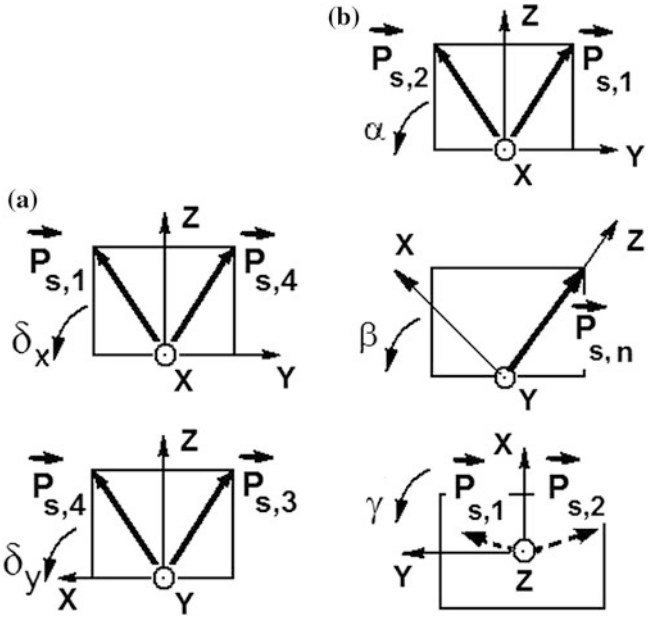

Fig. 3.3 Modes of rotation of the spontaneous polarisation vectors $\boldsymbol{P}_{s,1}$, $\boldsymbol{P}_{s,2}$, … in the [001]-poled (**a**) and [011]-poled (**b**) SCs. x, y and z are main crystallographic axes of the polydomain SCs, δ_x and δ_y are rotation angles for the [001]-poled SC, and α, β and γ are rotation angles for the [011]-poled SC (reprinted from paper by Topolov et al. [27], with permission from Taylor and Francis)

Because of the 4*mm* symmetry of the [001]-poled polydomain SC (see inset 2 in Fig. 1) and the equality of its piezoelectric coefficients $d_{31}^{(1)} = d_{32}^{(1)}$, we do not consider the rotation of the main crystallographic axes x, y and z around $OX_3 \parallel$ z in Composite-2.

The effective electromechanical properties and related parameters of the 2–2 SC/polymer composite are evaluated using (3.5) and complete sets of electromechanical constants of components (see Tables 3.4 and 3.5). Elements of the $\| C^* \|$ matrix from (3.5) are represented as functions of the volume fraction of SC m and rotation angles shown in Figs. 3.2 and 3.3.

By taking into account the symmetry features of the components (Tables 3.4 and 3.5) and the periodic laminar structure (Fig. 3.2), one can state the periodicity of the orientation dependence of the effective parameters of the 2–2 composite. For instance, its hydrostatic parameters obey equalities $\Pi_h^*(m, \varphi, \psi, \theta) = \Pi_h^*(m, 120° \pm \varphi, \psi, \theta)$ and $\Pi_h^*(m, \varphi, \psi, \theta) = \Pi_h^*(m, \varphi, 180° \pm \psi, \theta)$ for Composite-1, and $\Pi_h^*(m, \gamma) = \Pi_h^*(m, 180° \pm \gamma)$ for Composite-3 [27].

The squared hydrostatic figure of merit $\left(Q_h^*\right)^2$ from (3.6) strongly depends on the rotation mode of the main crystallographic axes (Table 3.6 and Fig. 3.3). Data from Table 3.6 enable us to conclude that Composite-3 is preferable due to the

Table 3.6 Absolute maxima of hydrostatic parameters Π_h^* of the 2–2 PMN–0.28PT SC/PVDF composite at various rotation modes of the main crystallographic axes in the SC layers

Π_h^*	Value of absolute maxΠ_h^*	Volume fraction m and orientation angles which correspond to the value of maxΠ_h^*
Composite-1		
d_h^*	133 pC/N	$m = 0.238$, $\varphi = 0°$, $\psi = 0°$, and $\theta = 74°$
g_h^*	242 mV m/N	$m = 0.007$, $\varphi = 60°$, $\psi = 90°$, and $\theta = 57°$
$\left(Q_h^*\right)^2$	$12.3 \cdot 10^{-12}$ Pa^{-1}	$m = 0.021$, $\varphi = 60°$, $\psi = 90°$, and $\theta = 63°$
Composite-2		
d_h^*	228 pC/N	$m = 0.253$ and $\delta_x = 0°$, or $m = 0.253$ and $\delta_y = 0°$
g_h^*	230 mV m/N	$m = 0.007$ and $\delta_x = 0°$, or $m = 0.007$ and $\delta_y = 0°$
$\left(Q_h^*\right)^2$	$15.3 \cdot 10^{-12}$ Pa^{-1}	$m = 0.038$ and $\delta_x = 0°$, or $m = 0.038$ and $\delta_y = 0°$
Composite-3		
d_h^*	372 pC/N	$m = 0.337$ and $\gamma = 90°$
g_h^*	284 mV m/N	$m = 0.012$ and $\gamma = 90°$
$\left(Q_h^*\right)^2$	$33.8 \cdot 10^{-12}$ Pa^{-1}	$m = 0.068$ and $\gamma = 90°$

largest maximum value of $\left(Q_h^*\right)^2$, the simplest orientation of the main crystallographic axes and the volume fraction of SC m that is more than 5% and can be achieved at manufacturing the composite sample. According to experimental data from Table 3.4, the squared hydrostatic figure of merit the [011]-poled PMN–0.28PT SC is $\left(Q_h^{(1)}\right)^2 = 0.719 \cdot 10^{-12}$ Pa^{-1}, i.e., by 47 times less than max$\left[\left(Q_h^*\right)^2\right]$ (Table 3.6) in Composite-3 based on this SC. Such a high hydrostatic parameter of Composite-3 is achieved due to the presence of the [011]-poled SC layers with an unusual combination of electromechanical constants that characterise the SC anisotropy. As seen from Table 3.4, the [011]-poled SC is characterised by elastic compliances that obey the untypical conditions $s_{11}^{(1),E} \approx s_{13}^{(1),E}$, $\left|s_{23}^{(1),E}\right| \approx 2.7\, s_{13}^{(1),E}$ and $s_{33}^{(1),E} \approx 2s_{13}^{(1),E}$, while the piezoelectric coefficients of this SC obey conditions $d_{33}^{(1)} \approx 1.9 d_{31}^{(1)}$ and $\left|d_{32}^{(1)}\right| \approx 2.6 d_{31}^{(1)}$. Variations of the rotation angles α and β (Fig. 3.3b) in the [011]-poled SC of Composite-3 would lead to values of maxΠ_h^* which are lower than those listed in Table 3.6. This fact is also an argument for the important role of the anisotropy of the electromechanical properties of the SC component in forming the hydrostatic piezoelectric response of the 2–2 composite.

It should be added for comparison that values of max d_h^*, max g_h^* and max $\left[\left(Q_h^*\right)^2\right]$ of the studied composites (Table 3.6) highlight their advantages over the conventional 2–2 PZT-type FC/polymer composites, for which typical values are max $d_h^* \approx$ (50–80) pC/N and max $g_h^* \approx$ (100–300) mV m/N [28]. It is also known that experimental values of max $\left[\left(Q_h^*\right)^2\right] \approx 5 \cdot 10^{-11}$ Pa^{-1} are related to a 2–2 PZT-type FC/polymer composite [15] with a specific orientation of the layers with

respect to the poling direction. Thus, the orientation effect in the piezo-active 2–2 composites plays the important role in achieving the large values of $\left(Q_h^*\right)^2$ that is important for hydroacoustic applications.

The second example to be discussed is concerned with a 2–2 SC/auxetic polymer composite. The auxetic polymer component is characterised by a negative Poisson's ratio, i.e., elastic compliances of the isotropic material are $s_{11}^{(n)} > 0$ and $s_{12}^{(n)} > 0$ (see Table 2.7)[1]. This elastic feature can influence the electromechanical properties and related parameters of the composite [29] in a wide volume-fraction range. Among the SC components, of interest are perovskite-type relaxor-ferroelectric $x\mathrm{Pb}(\mathrm{In}_{0.5}\mathrm{Nb}_{0.5})\cdot$ $\cdot\mathrm{O}_3 - y\mathrm{Pb}(\mathrm{Mg}_{1/3}\mathrm{Nb}_{2/3})\mathrm{O}_3 - (1-x-y)\mathrm{PbTiO}_3$ (PIN-x-y) SCs in the single-domain state [30] at room temperature (see, for instance, data in Table 3.7). The full set of

Table 3.7 Room-temperature elastic compliances s_{ab}^E (in 10^{-12} Pa^{-1}), piezoelectric coefficients d_{ij} (in pC/N) and relative dielectric permittivity $\varepsilon_{pp}^{\sigma}/\varepsilon_0$ of the single-domain PIN-0.24-0.49 SC ($3m$ symmetry) [30]

Electromechanical constant	Single-domain [111]-poled PIN-0.24-0.49 SC
$s_{11}^{(n),E}$	11.62
$s_{12}^{(n),E}$	–7.81
$s_{13}^{(n),E}$	–1.10
$s_{14}^{(n),E}$	22.17
$s_{22}^{(n),E}$	11.62
$s_{23}^{(n),E}$	–1.10
$s_{33}^{(n),E}$	6.05
$s_{44}^{(n),E}$	93.33
$s_{55}^{(n),E}$	93.33
$s_{66}^{(n),E}$	38.85
$d_{15}^{(n)}$	2015
$d_{22}^{(n)}$	–490
$d_{24}^{(n)}$	2015
$d_{31}^{(n)}$	–21
$d_{32}^{(n)}$	–21
$d_{33}^{(n)}$	75
$\varepsilon_{11}^{(n),\sigma}/\varepsilon_0$	5800
$\varepsilon_{22}^{(n),\sigma}/\varepsilon_0$	5800
$\varepsilon_{33}^{(n),\sigma}/\varepsilon_0$	650

[1]For auxetic polyethylene it is assumed that its dielectric permittivity equals 2.3 as is known for monolithic polyethylene samples [31].

electromechanical constants of the single-domain PIN-0.24-0.49 SC testifies to the obvious anisotropy of its properties.

It is assumed that the 2–2 single-domain PIN-0.24-0.49 SC/auxetic polyethylene is characterised by the regular arrangement of layers as shown in Fig. 3.2. We use the Euler angles φ, ψ and θ to describe the rotation of the main crystallographic axes $\left(X_1^o X_2^o X_3^o\right) \rightarrow \left(X_1' X_2' X_3'\right)$ and the orientation of the spontaneous polarisation vector $\boldsymbol{P}_s^{(1)}$ in each single-domain SC layer (see inset 1 in Fig. 3.2). In the studied 2–2 composite based on the single-domain PIN-0.24-0.49 SC, large values of absolute maxima of g_h^* and $\left(Q_h^*\right)^2$ are achieved at very low volume fractions of SC: absolute max g_h^* = 3860 mV m/N at m = 0.0008 and absolute max $\left[\left(Q_h^*\right)^2\right] = 1.71 \cdot 10^{-9}$ Pa^{-1} at m = 0.0014 [29]. This performance is accounted for by the large elastic compliances of the auxetic component (see Table 3.7) in comparison to the elastic compliances of the SC component and by the effect of the dielectric properties of the auxetic component on the non-monotonic behaviour of g_h^* and $\left(Q_h^*\right)^2$ at $m << 1$. It is obvious that the aforementioned values of $m < 0.01$ do not enable one to create a composite sample with the extremely large value of $\left(Q_h^*\right)^2$. To avoid this limitation, we should consider the performance of this composite at larger volume fractions of SC.

Examples of the behaviour of $\left(Q_h^*\right)^2$ in vicinities of local maxima achieved at variations of the Euler angles are shown in Fig. 3.4. The considerable decrease of $\left(Q_h^*\right)^2$ in comparison to the values of absolute max $\left[\left(Q_h^*\right)^2\right] = 1.71 \cdot 10^{-9}$ Pa^{-1} [29] is concerned with the increase of dielectric permittivity $\varepsilon_{33}^{*\sigma}$ that strongly influences

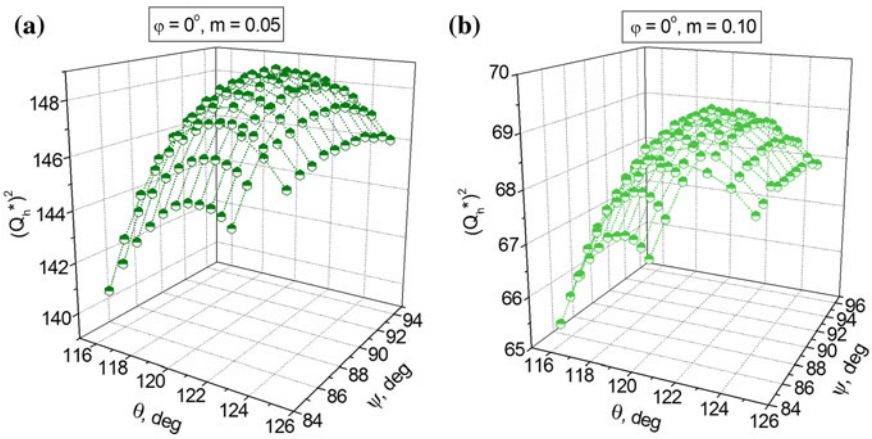

Fig. 3.4 Hydrostatic squared figure of merit $\left(Q_h^*\right)^2$ (in 10^{-12} Pa^{-1}) of the 2–2-type PIN-0.24-0.49/auxetic polyethylene composite in the vicinity of local max $\left[\left(Q_h^*\right)^2\right]$ at m = 0.05 (**a**) and m = 0.10 (**b**) (reprinted from paper by Topolov et al. [29], with permission from Wiley-VCH)

[7, 10] the piezoelectric coefficients g_{33}^* and g_h^* and, therefore, $\left(Q_h^*\right)^2$ in accordance with (3.6). At volume fractions of SC $0.05 \le m \le 0.10$, irrespective of the orientation of the main crystallographic axes in the SC layer, the inequality $\varepsilon_{33}^{*\sigma} \ll \varepsilon_{33}^{(1),\sigma}$ holds, and this feature of the composite favours relatively large values of $g_h^* \sim 10^2$ mV m/N and $\left(Q_h^*\right)^2 \sim 10^{-11}$–$10^{-10}$ Pa^{-1} [29] which are of interest for hydroacoustic applications.

The third example of the performance is concerned with local maxima of squared figures of merit $\left(Q_{33}^*\right)^2$ and $\left(Q_h^*\right)^2$. These parameters were analysed for a 2–2-type polydomain PMN–*x*PT SC/auxetic polyethylene composite [32] with x = 0.28–0.33. As a result of the complicated microgeometry of the auxetic polymer component, we use the notation '2–2-type' instead of '2–2'. As follows from Fig. 3.5, the squared figures of merit $\left(Q_{33}^*\right)^2$ and $\left(Q_h^*\right)^2$ decrease with an increase in the volume fraction of SC m. However values of local maxima of both $\left(Q_{33}^*\right)^2$ and $\left(Q_h^*\right)^2$ at $0.05 < m < 0.2$ are still large in comparison to the similar values related to the conventional 2–2 FC/polymer composites [7, 14, 15]. The considerable anisotropy of the electromechanical properties of the SC component and the unusual elastic properties of the polymer component promote the anisotropy of figures of merit which correspond to the longitudinal and transverse piezoelectric responses of the composite. The inequality

$$\left(Q_{33}^*\right)^2 / \left(Q_{3j}^*\right)^2 \ge 10 \; (j = 1 \text{ and } 2) \tag{3.8}$$

holds [32] within wide ranges of m and rotation angles (Fig. 3.6) and at different rotation modes. The considerable part of the hatched area in Fig. 3.6a is related to the volume fraction m and orientation angle α that promote large values of $\left(Q_h^*\right)^2$.

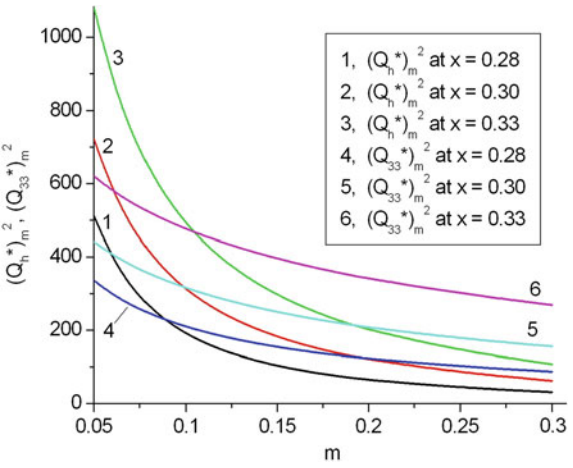

Fig. 3.5 Local maxima of squared figures of merit $\left(Q_h^*\right)m^2$ and $\left(Q_{33}^*\right)m^2$ (in 10^{-12} Pa^{-1}) of the 2–2-type PMN–*x*PT SC/auxetic polyethylene composite with SC layers poled along [001] (reprinted from paper by Bowen and Topolov [32], with permission from Taylor and Francis)

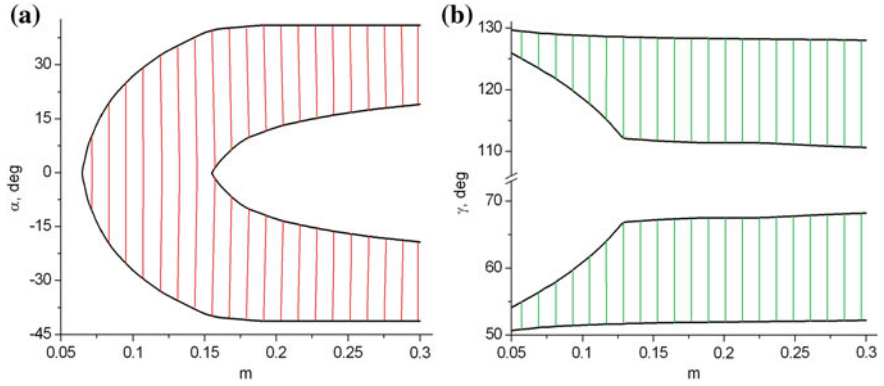

Fig. 3.6 Examples of validity of condition (3.8) (hatched areas in graphs) at different rotation modes in the 2–2-type PMN–*x*PT SC/auxetic PE composite: a, $x = 0.33$ and SC layers poled along [001], and b, $x = 0.29$ and SC layers poled along [011] (reprinted from paper by Bowen and Topolov [32], with permission from Taylor and Francis)

The rotation mode concerned with α is shown in Fig. 3.3b. We note that the validity of the condition (3.8) is linked with the appreciable orientation effect and elastic anisotropy of the studied composite and the relatively high piezoelectric activity of its SC component irrespective of its poling direction. It is clear that condition (3.8) is similar to (3.2) related to the $PbTiO_3$-type FCs with a large piezoelectric anisotropy. However the condition (3.8) was formulated [32] for 2–2 composites based on PMN–*x*PT SCs with large piezoelectric coefficients $d_{3j}^{(1)}$.

Thus, the results shown in Sect. 3.2 enable us to characterise the piezo-active 2–2 composites as materials with figures of merit that can vary in wide ranges. Of particular interest are the 2–2 composites based on relaxor-ferroelectric SCs that are poled along specific directions and promote the high piezoelectric activity and sensitivity of the composites.

3.3 1–3 Composites

In the 1–3 composite, the main piezo-active component is self-connected in one dimension (often along the poling axis) and the piezo-passive component (or the component with a low piezoelectric activity) is self-connected in three dimensions. In fact, it is a system of long aligned poled rods embedded in a large matrix. The 1–3 FC/polymer and relaxor-ferroelectric SC/polymer composites (Figs. 2.2 and 2.3) are widespread [7, 8, 10, 14, 15, 19, 20] due to the ease of poling and a variety of advantages over the poled monolithic piezo-active components. Often the FC component can be represented by a continuous row of particles, relatively long rods or fibres, or a series of discs. The cross-section of the FC rod can be in the form of a

square, circle, ellipse, triangle, etc. The combination of the relatively low dielectric permittivity and high piezoelectric activity at small volume fractions of the FC or SC component results in a significant piezoelectric sensitivity of the 1–3 composite [7, 19, 20]. The 1–3 relaxor-ferroelectric SC/polymer composite is of interest due to the combination of the high piezoelectric activity and sensitivity, considerable electromechanical coupling, hydrostatic piezoelectric response, etc. Orientation effects studied in such a composite [10] represent an independent interest at improving the performance in comparison to the traditional FC/polymer composites. Undoubtedly, advantages of the 1–3 composites over individual FC or SC components stimulate intensive research into the development and manufacture of 1–3 and related piezo-active composites in the last decades. An additional stimulus is achieved by modification of the polymer matrix; see, for instance, [10, 33–35].

In Sect. 3.3 we analyse examples of figures of merit and ways to increase these parameters in the 1–3 and related composites based on either FCs or domain-engineered relaxor-ferroelectric SCs.

3.3.1 Ceramic/Polymer Composites

We assume that the 1–3 composite consists of long FC rods (component 1) that are regularly distributed in a continuous polymer matrix (component 2). The rods are considered to be in the form of circular cylinders aligned parallel to the poling OX_3 axis and continuous in the same direction (Fig. 3.7). In the (X_1OX_2) plane, a square arrangement of the cylinders is formed.

The effective electromechanical properties of the 1–3 composite are represented in the general form [7, 10] as

$$||C^*|| = \left|\left|C^{(2)}\right|\right| + m\left(\left|\left|C^{(1)}\right|\right| - \left|\left|C^{(2)}\right|\right|\right)||A||. \tag{3.9}$$

In (3.9), $\left|\left|C^{(n)}\right|\right| = \begin{pmatrix} \left|\left|C^{(n),E}\right|\right| & \left|\left|e^{(n)}\right|\right|^t \\ \left|\left|e^{(n)}\right|\right| & -\left|\left|\varepsilon^{(n),\xi}\right|\right| \end{pmatrix}$ is the 9×9 matrix that characterises the electromechanical properties of the FC rod (at $n = 1$) and the surrounding polymer

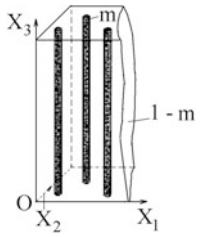

Fig. 3.7 Schematic of the 1–3 composite with cylindrical rods. m and $1 - m$ are volume fractions of the FC rods and the polymer matrix, respectively. $(X_1X_2X_3)$ is the rectangular co-ordinate system (reprinted from monograph by Topolov and Bowen [7], with permission from Springer)

matrix (at $n = 2$), is the mechanical strain—electric field concentration matrix (9×9 matrix), $\| c^{(n),E} \|$ is the 6×6 matrix of elastic moduli measured at constant electric field, $\| e^{(n)} \|$ is the 6×3 matrix of piezoelectric coefficients, $\| \varepsilon^{(n),\xi} \|$ is the 3×3 matrix of dielectric permittivities measured at mechanical strain $\xi = \text{const}$, and superscript 't' denotes the transposition. The $\| A \|$ matrix from (3.9) is related to the boundary conditions in the 'rod—surrounding medium' region. Taking into account an electromechanical interaction between the piezo-active rods in the composite and following the effective field method [7, 10, 36, 37], we write $\| A \|$ as

$$||A|| = \left[||I|| + (1-m)\|S\|\left\|C^{(2)}\right\|^{-1}\left(\left\|C^{(1)}\right\| - \left\|C^{(2)}\right\|\right)\right]^{-1}. \tag{3.10}$$

In (3.10), $\| I \|$ is the 9×9 identity matrix, and $\| S \|$ is the 9×9 matrix containing components of the Eshelby electroelastic tensor [37–39]. Elements of $\| C^* \|$ from (3.9) are functions of the volume fraction m. Taking into account the square arrangement of the rods the ($X_1 O X_2$) plane (Fig. 3.7), we note that the upper limit for their volume fraction would be $\pi/4$. A transition from the full set of electromechanical constants, that constitute $\| C^* \|$, to the piezoelectric coefficients d_{ij}^*, g_{ij}^*, squared figures of merit from (3.6), etc. is carried out using conventional formulae [11, 12] for the piezoelectric medium.

As is known [7, 35], values of $\max \left[Q_{33}^*(m)\right]^2$ and $\max \left[Q_h^*(m)\right]^2$ in the 1–3 composite based on the PZT-type FC, are several tens of times larger than the $\left[Q_{33}^*(1)\right]^2$ and $\left[Q_h^*(1)\right]^2$ values related to the monolithic FC component. As a rule, $\max \left[Q_{33}^*(m)\right]^2$ and $\max \left[Q_h^*(m)\right]^2$ are attained at relatively small volume fractions of the PZT-type FC, i.e., at $0 < m < 0.1$ [7, 35]. In the same m range, the 1–3 composite is characterised by a large anisotropy of the piezoelectric coefficients e_{3j}^*, i.e., $e_{33}^* / \left|e_{31}^*\right| \gg 1$. Taking into account these results, we represent (3.6) in the form [35]

$$\begin{aligned} &(Q_h^*)^2 \approx \eta_{elas,h}^* \left(e_{33}^* / c_{33}^{*E}\right)^2 / \varepsilon_{33}^{*\sigma} \approx \eta_{elas,h}^* \left[m\, e_{33}^{(1)} / \left(m c_{33}^{(1),E} + c_{33}^{(2),E}\right)\right]^2 / \left(m\, \varepsilon_{33}^{(1),\sigma}\right) \\ &\text{and } \left(Q_{33}^*\right)^2 \approx \left(\eta_{elas,33}^* / \eta_{elas,h}^*\right)(Q_h^*)^2. \end{aligned} \tag{3.11}$$

In (3.11), $\eta_{elas,h}^* = \left\{\left[1 + \left(\beta_{12}^*\right)^{-1} - 2\left(\beta_{13}^*\right)^{-1}\right] / \left[1 + \left(\beta_{12}^*\right)^{-1} - 2\left(\beta_{13}^*\right)^{-1}\left(\beta_{33}^* / \beta_{13}^*\right)\right]\right\}^2$, $\eta_{elas,33}^* = \left\{\left[1 + \left(\beta_{12}^*\right)^{-1}\right] / \left[1 + \left(\beta_{12}^*\right)^{-1} - 2\left(\beta_{13}^*\right)^{-1}\left(\beta_{33}^* / \beta_{13}^*\right)\right]\right\}^2$ and $\beta_{ab}^* = c_{11}^{*E} / c_{ab}^{*E}$ depend on the elastic properties of the composite only, and an inequality $e_{33}^{(1)} \gg e_{33}^{(2)}$ holds for its components. $(Q_h^*)^2$ and $(Q_{33}^*)^2$ from (3.11) depend on

$\gamma = me_{33}^{(1)} / \left(mc_{33}^{(1),E} + c_{33}^{(2),E} \right)$, so that a higher $e_{33}^{(1)} / c_{33}^{(1),E}$ ratio leads to larger $(Q_h^*)^2$ and $(Q_{33}^*)^2$ at $0 < m < 0.1$.

We note that among the perovskite-type FCs listed in Table 1.2 and C.1, PCR-7M is characterised by the highest $e_{33}^{(1)} / c_{33}^{(1),E}$ ratio at room temperature. For example, max $\left[Q_h^*(m)\right]^2 = 6.24 \cdot 10^{-12}$ Pa^{-1} and max $\left[Q_{33}^*(m)\right]^2 = 6.24 \cdot 10^{-10}$ Pa^{-1} are achieved in the 1–3 PCR-7M/elastomer composite [35]. The max $\left[Q_h^*(m)\right]^2$ value is approximately three times larger than that of typical 1–3 composites based on the PZT-type FCs [7, 14].

Data on the piezoelectric properties and squared figures of merit of the studied composites based on FCs are shown in Table 3.8. It is seen that values of $(Q_{3j}^*)^2$ of the PZT-5-based composite are comparable to $(Q_{3j}^*)^2$ of the 2–2 composite with the same components (see Table 3.8). The $(Pb_{0.75}Ca_{0.25})TiO_3$ FC belongs to the highly anisotropic $PbTiO_3$-type FCs [40] and does not give rise to large values of $(Q_{3j}^*)^2$ in the related 1–3 composite. The combination of the PCR-7M FC (i.e., soft ferroelectric material with large values of $d_{33}^{(1)}$ and $\left|d_{31}^{(1)}\right|$ [9]) and auxetic polyethylene leads to very large values of $(Q_{33}^*)^2$ at non-monotonic changes in $(Q_{31}^*)^2$. These changes are caused by decreasing d_{31}^* in the wide m range and by changing sgn d_{31}^* (see Table 3.8). The 1–3-type PCR-7M FC/auxetic polyethylene composite is also of interest due to the relatively large volume-fraction range wherein condition (3.8) for the large anisotropy of $(Q_{3j}^*)^2$ is valid. This is a result of the active role of the auxetic,namely, its unusual elastic properties, in forming the piezoelectric properties and their considerable anisotropy [33] in the studied composite.

3.3.2 *Single Crystal/Polymer Composites*

The 1–3 relaxor-ferroelectric SC/polymer composite is of interest for various piezotechnical applications, including piezoelectric energy harvesting [19, 20]. The SC component with large piezoelectric coefficients $d_{3j} \sim 10^3$ pC/N (see Table 1.1) favours the strong electromechanical coupling (see Sect. 2.5.2), high piezoelectric sensitivity and activity, etc. [7, 42]. Taking the domain-engineered SC component, one can form the structure of the SC rods that are regularly arranged in the continuous polymer matrix (Fig. 2.4) and strongly influence the piezoelectric properties in the composite system. By varying the volume fraction of the SC rods m, one can tailor a composite sample with effective parameters near their extreme points that are predicted by various methods [7]. Taking into account a rotation of the main crystallographic axes in each SC rod and the related orientation effect [10, 43], one can improve the piezoelectric response and related parameters of the 1–3 composite. A modification of the polymer matrix, for instance by forming a porous

Table 3.8 Volume-fraction dependences of the piezoelectric coefficients d_{3j}^{*} (in pC/N), g_{3j}^{*} (in mV m/N) and squared figures of merit $\left(Q_{3j}^{*}\right)^{2}$ (in 10^{-12} Pa^{-1}), which have been calculated for the 1–3-type composites with cylindrical rods

m	d_{31}^{*}	d_{33}^{*}	g_{31}^{*}	g_{33}^{*}	$\left(Q_{31}^{*}\right)^{2}$	$\left(Q_{33}^{*}\right)^{2}$
1–3 PZT-5 FC/araldite composite						
0	0	0	0	0	0	0
0.05	–52.8	141	–56.1	150	2.96	21.2
0.1	–79.6	210	–40.1	106	3.19	22.3
0.2	–108	277	–25.7	65.9	2.78	18.3
0.3	–124	310	–19.1	47.8	2.37	14.8
0.4	–135	330	–15.4	37.6	2.08	12.4
0.5	–143	343	–12.9	30.9	1.84	10.6
0.6	–150	353	–11.2	26.4	1.68	9.32
1–3 $(Pb_{0.75}Ca_{0.25})TiO_3$ FC/araldite composite [40]						
0	0	0	0	0	0	0
0.05	–7.28	19.9	–69.1	189	0.503	3.76
0.1	–6.73	22.0	–38.4	126	0.258	2.77
0.2	–6.65	25.0	–21.1	79.3	0.140	1.98
0.3	–5.99	26.1	–13.1	57.3	0.0785	1.50
0.4	–5.19	26.8	–8.69	44.9	0,0451	1.19
0.5	–4.35	27.2	–5.89	36.9	0.0256	0.893
0.6	–3.51	27.4	–3.99	31.2	0.0140	0.855
1–3-type PCR-7M FC/auxetic polyethylene composite [33]						
0	0	0	0	0	0	0
0.05	415	669	193	310	80.1	207
0.1	318	698	72.4	158	23.0	110
0.2	153	718	17.1	80.3	2.62	57.7
0.3	30.1	729	2.23	53.9	0.0671	39.3
0.4	–64.7	736	–3.57	40.5	0.231	29.8

(continued)

Table 3.8 (continued)

m	d_{31}^*	d_{33}^*	g_{31}^*	g_{33}^*	$\left(Q_{31}^*\right)^2$	$\left(Q_{33}^*\right)^2$
0.5	–141	741	–6.20	32.5	0.874	24.1
0.6	–206	745	–7.53	27.2	1.55	20.3

Notes

1. The full set of room-temperature electromechanical constants of the $(Pb_{0.75}Ca_{0.25})TiO_3$ FC was taken from work [41]. Elastic and dielectric constants of auxetic polyethylene were taken from Table 2.7
2. The effective field method was used to calculate the effective electromechanical properties of the 1–3 PZT-5 FC/araldite and $(Pb_{0.75}Ca_{0.25})TiO_3$ FC/araldite composites
3. The finite element method was used to calculate the effective electromechanical properties of the 1–3-type PCR-7M FC/auxetic polyethylene composite
4. For the $(Pb_{0.75}Ca_{0.25})TiO_3$ FC/araldite composite, differences between the effective parameters calculated using the effective field method and those calculated by means of the finite element method are less than 3 % [40]
5. We do not consider specifics of connectivity of the PCR-7M FC/auxetic polyethylene composite because of complicated microgeometry of the auxetic polymer matrix, and hereafter the notation '1–3-type' is used

structure therein [42] or incorporating FC inclusions therein [44–46], provides additional opportunities to improve composite performance.

Squared figures of merit $\left(Q_{33}^*\right)^2$ and $\left(Q_h^*\right)^2$ of the 1–3 composite based on the relaxor-ferroelectric domain-engineered [001]-poled SC vary in wide ranges (curve 1 in Fig. 3.8), however their maxima are observed at relatively small volume fractions on SC, $m \approx 0.1$–0.2. Values of $\left(Q_{33}^*\right)^2$ near its maximum (see curve 1 in Fig. 3.8a) are about 7–10 times more than $\left(Q_{33}^*\right)^2$ of the 1–3 PZT-5 FC/araldite composite and comparable to $\left(Q_{33}^*\right)^2$ of the 1–3-type PCR-7M FC/auxetic polyethylene composite (see Table 3.8). By replacing the monolithic polymer matrix with a porous polymer matrix, wherein the spherical air pores are distributed regularly, we achieve larger values of $\left(Q_{33}^*\right)^2$ and $\left(Q_h^*\right)^2$ without considerable shifts of their maximum points (curve 2 in Fig. 3.8). This is due to the active role of the elastic properties of the matrix at its dielectric permittivity $\varepsilon_{33}^{(2)} \ll \varepsilon_{33}^{*\sigma}$. Values of $\left(Q_h^*\right)^2 \approx 6 \cdot 10^{-12}$ Pa^{-1} (curve 1 in Fig. 3.8b) are more than $\left(Q_h^*\right)^2$ of a 1–3–0 PZT rod composite [14] and close to max $\left(Q_h^*\right)^2$ of the 1–3 PCR-7M/elastomer composite [35]. Values of $\left(Q_h^*\right)^2 \approx 25 \cdot 10^{-12}$ Pa^{-1} (curve 2 in Fig. 3.8b) exceed $\left(Q_h^*\right)^2$ of such FC-based materials as 1–3–0 PZT rods—foamed polymer and 3–2 perforated composites [14].

Large values of both $\left(Q_{33}^*\right)^2$ and $\left(Q_h^*\right)^2$ are achieved in the novel 1–3-type lead-free composites at relatively small volume fractions of SC m (Fig. 3.9). Such a

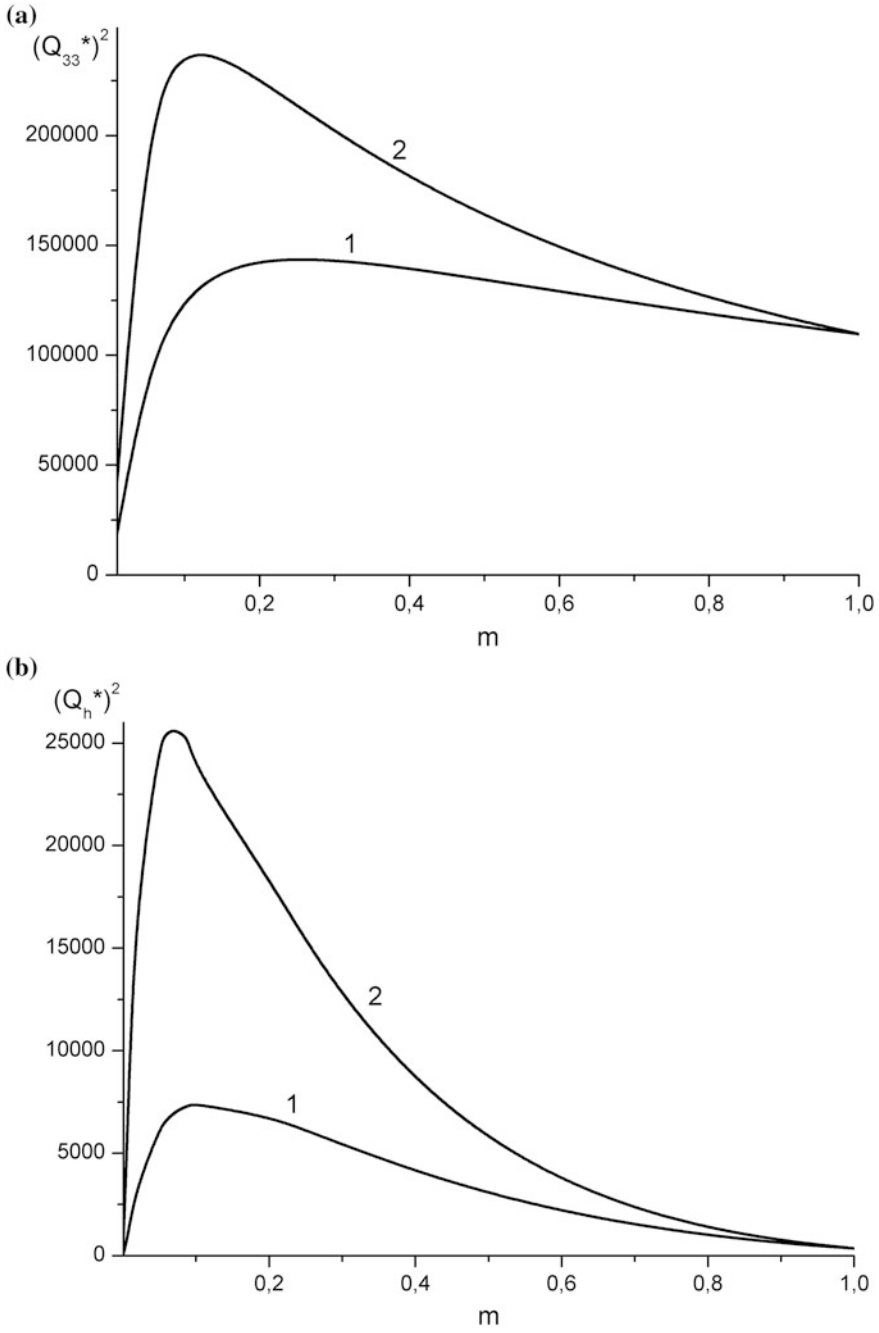

Fig. 3.8 Volume-fraction dependences of squared figure of merit $\left(Q_{33}^*\right)^2$ (**a** in 10^{-15} Pa^{-1}), and squared hydrostatic figure of merit $\left(Q_h^*\right)^2$ (**b** in 10^{-15} Pa^{-1}) that have been calculated for the following 1–3-type composites: PMN–0.33PT SC/araldite (curve 1) and PMN–0.33PT SC/porous araldite at the volume fraction $m_p = 0.3$ of spherical air pores (curve 2) (reprinted from Bezus et al. [42], with permission from IOP Publishing)

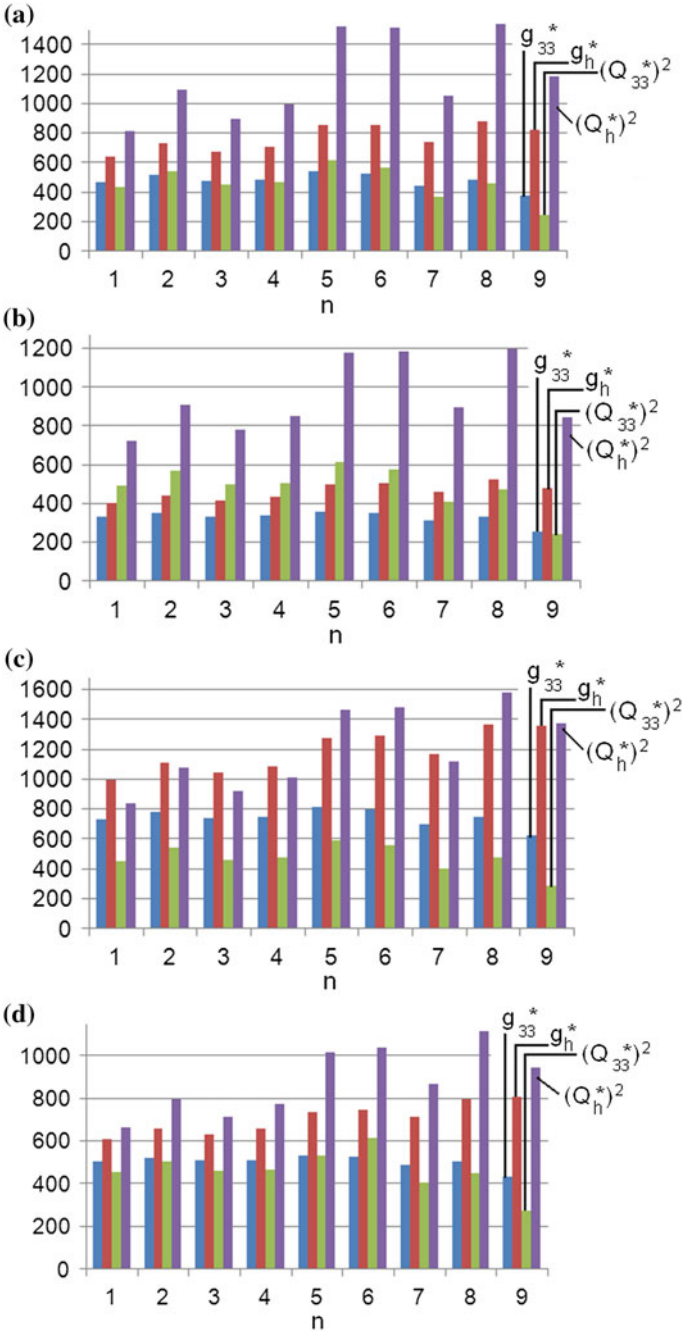

Fig. 3.9 Piezoelectric coefficients g_{33}^* and g_h^* (in mV m/N) and squared figures of merit $\left(Q_{33}^*\right)^2$ and $\left(Q_h^*\right)^2$ (in 10^{-13} Pa^{-1}) of 1–3-type KNN-TL SC/auxetic PE-*n* (graphs **a** and **c**) and KNN-T SC/auxetic PE-*n* (graphs **b** and **d**) composites at volume fractions of SC $m = 0.05$ (graphs **a** and **b**) and $m = 0.10$ (graphs **c** and **d**) (reprinted from paper by Topolov and Bowen [47], with permission from Elsevier)

performance is accounted for by the role of the elastic properties of the auxetic polymer component at its dielectric permittivity $\varepsilon_{33}^{(2)} \ll \varepsilon_{33}^{*\sigma}$. At $m \leq 0.1$, the dielectric permittivity of the 1–3-type composite obeys the condition $\varepsilon_{33}^{*\sigma} \ll \varepsilon_{33}^{(1)}$ that promotes large piezoelectric coefficients g_{33}^{*} and g_{h}^{*} and strongly influences the squared figures of merit $\left(Q_{33}^{*}\right)^2$ and $\left(Q_{h}^{*}\right)^2$ in accordance with (3.6).

3.4 0–3 Composites

Because of the system of isolated piezoelectric inclusions in a continuous matrix (Fig. 2.7), the 0–3 composite is characterised by moderate figures of merit. Despite the presence of the very prolate FC inclusions oriented along the poling axis OX_3, values of $\left(Q_{3j}^{*}\right)^2$ and $\left(Q_{h}^{*}\right)^2$ of the 0–3 composite based on the FC with a high piezoelectric activity are less than those of the related 1–3 composite [35]. The values of $\left(Q_{3j}^{*}\right)^2$ and $\left(Q_{h}^{*}\right)^2$ of the 0–3 PCR-7M FC/araldite composite (Table 3.9) are also less than $\left(Q_{3j}^{*}\right)^2$ and $\left(Q_{h}^{*}\right)^2$ of the 1–3-type PCR-7M FC/auxetic polyethylene composite; however they are comparable to $(Q_{3j}^{*})^2$ and $(Q_{h}^{*})^2$ of the 1–3 PZT-5 FC/araldite composite (Table 3.8). Despite the relatively large piezoelectric coefficient $g_{33}^{(1)}$ of the FC component, the 0–3 $(Pb_{0.75}Ca_{0.25})TiO_3$ FC/araldite composite is characterised by small values of $\left(Q_{3j}^{*}\right)^2$ and $\left(Q_{h}^{*}\right)^2$ in comparison to the 0–3 PCR-7M FC/araldite composite (Table 3.9). Decreasing $\left(Q_{3j}^{*}\right)^2$ and $\left(Q_{h}^{*}\right)^2$ from (3.6) may be due to the polymer (its elastic properties) or FC (its piezoelectric activity).

The 0–3 PMN–0.33PT SC/araldite composite with prolate inclusions exhibits high values of $\left(Q_{3j}^{*}\right)^2$ at $\rho = 0.1$ (Table 3.9), and increasing the aspect ratio ρ gives rise to an appreciable decrease of $\left(Q_{3j}^{*}\right)^2$ and $\left(Q_{h}^{*}\right)^2$. This effect observed in the presence of a SC component with high piezoelectric activity (see d_{3j} in Table 1.1) and is accounted for by the influence of the shape of inclusions on the piezoelectric properties of the 0–3 composite [7]. An increase of ρ leads to the effect of the depolarising field of the inclusion on the effective electromechanical properties of the 0–3 composite, and as a consequence, its piezoelectric activity decreases with increasing ρ.

The next example of the volume-fraction dependence of the squared figures of merit $\left(Q_{3j}^{*}\right)^2$ and $\left(Q_{h}^{*}\right)^2$ of composites based on the PMN–0.33PT SC is shown in

Table 3.9 Volume-fraction dependences of the piezoelectric coefficients d_{3j}^* (in pC/N), g_{3j}^* (in mV m/N) and squared figures of merit $\left(\left(Q_{3j}^*\right)^2\right.$ and $\left(Q_h^*\right)^2$ (in 10^{-12} Pa^{-1}), which have been calculated for the 0–3 composites with spheroidal piezoelectric inclusions

m	d_{31}^*	d_{33}^*	g_{31}^*	g_{33}^*	$\left(Q_{31}^*\right)^2$	$\left(Q_{33}^*\right)^2$	$\left(Q_h^*\right)^2$
PCR-7M FC/araldite composite, aspect ratio ρ = 0.01							
0	0	0	0	0	0	0	0
0.05	–98.5	268	–70.9	193	6.98	51.7	3.64
0.1	–151	405	–46.1	124	6.96	50.2	3.28
0.2	–210	544	–27.8	72.0	5.84	39.2	2.03
0.3	–244	614	–20.0	50.3	4.88	30.9	1.30
0.4	–267	657	–15.8	38.9	4.22	25.6	0.898
0.5	–286	686	–13.2	31.7	3.78	21.7	0.604
$(Pb_{0.75}Ca_{0.25})TiO_3$ FC/araldite composite, aspect ratio ρ = 0.01							
0	0	0	0	0	0	0	0
0.1	–6.58	21.5	–38.0	124	0.250	2.67	0.400
0.2	–6.54	24.6	–21.0	78.7	0.137	1.94	0.423
0.3	–5.90	25.8	–13.1	57.1	0.0773	1.47	0.433
0.4	–5.12	26.5	–8.66	44.8	0.0443	1.19	0.447
0.5	–4.30	26.9	–5.88	36.8	0.0253	0.990	0.458
PMN–0.33PT SC/araldite composite, aspect ratio ρ = 0.1 [48]							
0	0	0	0	0	0	0	0
0.05	–15.0	39.4	–94.7	249	1.42	9.81	0.542
0.1	–27.2	70.1	–81.9	211	2.23	14.8	0.741
0.2	–47.8	118	–59.1	146	2.82	17.2	0.614
0.3	–67.5	161	–46.3	110	3.13	17.7	0.452
0.4	–89.9	207	–38.5	88.6	3.46	18.3	0.316
0.5	–121	267	–33.6	73.8	4.07	19.7	0.165
PMN–0.33PT SC/araldite composite, aspect ratio ρ = 0.3 [48]							
0	0	0	0	0	0	0	0
0.05	–1.51	3.68	–26.2	63.9	0.0396	0.235	$7.59 \cdot 10^{-3}$
0.1	–3.04	7.25	–35.7	85.1	0.109	0.617	$1.06 \cdot 10^{-2}$
0.2	–6.01	13.8	–38.6	88.8	0.232	1.23	$2.06 \cdot 10^{-2}$
0.3	–9.12	20.4	–36.2	81.0	0.330	1.65	$1.86 \cdot 10^{-2}$
0.4	–13.0	28.3	–33.5	72.7	0.436	2.06	$1.31 \cdot 10^{-2}$
0.5	–20.5	43.1	–31.4	66.0	0.644	2.84	$6.72 \cdot 10^{-3}$
PMN–0.33PT SC/araldite composite, aspect ratio ρ = 0.5 [48]							
0	0	0	0	0	0	0	0
0.05	–0.570	1.31	–12.3	28.2	0.00701	0.0369	$7.20 \cdot 10^{-4}$
0.1	–1.19	2.68	–20.0	44.9	0.0238	0.120	$1.47 \cdot 10^{-3}$
0.2	–2.50	5.48	–27.1	59.3	0.0678	0.325	$2.45 \cdot 10^{-3}$

(continued)

Table 3.9 (continued)

m	d_{31}^*	d_{33}^*	g_{31}^*	g_{33}^*	$\left(Q_{31}^*\right)^2$	$\left(Q_{33}^*\right)^2$	$\left(Q_h^*\right)^2$
0.3	–3.99	8.57	–29.0	62.4	0.116	0.535	$2.60 \cdot 10^{-3}$
0.4	–5.97	12.7	–29.1	61.6	0.173	0.764	$2.58 \cdot 10^{-3}$
0.5	–10.3	22.0	–29.8	61.4	0.307	1.35	$5.32 \cdot 10^{-3}$

Notes

1. The effective piezoelectric coefficients and squared figures of merit of the PCR-7M FC/araldite composite and $(Pb_{0.75}Ca_{0.25})TiO$ FC/araldite composites were evaluated by means of the effective field method [7, 10]
2. The effective piezoelectric coefficients and squared figures of merit of the PMN–0.33PT SC/araldite composite were evaluated using the finite element method [10, 49]

Fig. 3.10. Changes in $\left(Q_h^*\right)^2$ are observed in relatively narrow ranges (see curves 2, 4 and 6 in Fig. 3.10) irrespective of the components, while $\left(Q_{33}^*\right)^2$ can vary in wide ranges (see curves 1, 3 and 5 in Fig. 3.10). In our opinion, this behaviour is concerned with the important role of the matrix, its piezoelectric activity and anisotropy. It is also seen that the non-monotonic behaviour of $\left(Q_h^*\right)^2$ (see curve 2 in Fig. 3.10) is observed in the composite with the polymer matrix only. Replacing such a matrix with a FC or porous FC matrix leads to monotonic increasing $\left(Q_h^*\right)^2$ (see curves 4 and 6 in Fig. 3.10). It should be added that values of $\left(Q_h^*\right)^2$ from Fig. 3.10 exceed those related to the 0–3 $PbTiO_3$-based and 1–3–0 PZT rod composites [14].

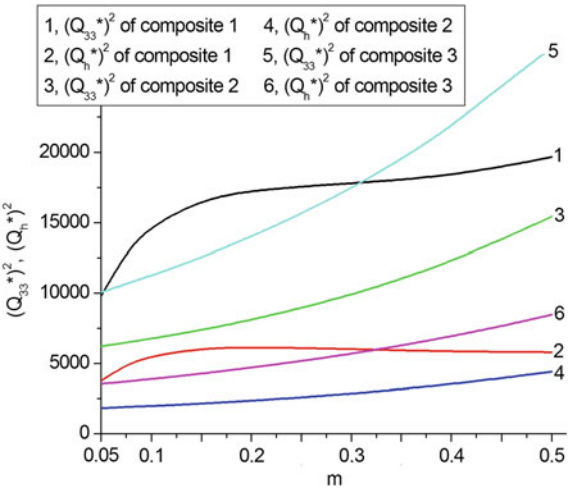

Fig. 3.10 Squared figures of merit $\left(Q_{33}^*\right)^2$ and $\left(Q_h^*\right)^2$ (in 10^{-15} Pa^{-1}) which have been calculated using the finite element method data on piezoelectric coefficients d_{3j}^* and g_{3j}^* of the following 0–3-type composites with spheroidal SC inclusions at their aspect ratio $\rho = 0.1$: PMN–0.33PT SC/araldite (termed 'composite 1'), PMN–0.33PT SC/PMN–0.35PT FC (termed 'composite 2') and PMN–0.33PT SC/porous PMN–0.35PT FC at the volume fraction $m_p = 0.3$ of spherical air pores (termed 'composite 3') (reprinted from paper by Topolov et al. [49], with permission from Taylor and Francis)

3.5 New Effects and Improved Figures of Merit in 1–3-Type Composites Based on Relaxor-Ferroelectric Single Crystals

3.5.1 New Orientation Effect

In Sect. 3.5.1 the influence of the mutual orientation of the poling directions of relaxor-ferroelectric SC and FC components on the electromechanical properties and related parameters of the 1–3-type composites is considered. These composites comprise two ferroelectric components with different polarisation directions and appreciable differences in their electromechanical properties, which lead to a *new orientation effect* [44] and improve the effective parameters. This additional improvement is of an independent interest because of complex inter-relationships in the fundamental triangle [7] of 'composition—structure—properties'.

It is assumed that the composite consists of long SC rods embedded in a heterogeneous matrix (Fig. 3.11a). The SC rods are in the form of the rectangular parallelepiped with a square base and square arrangement in the (X_1OX_2) plane. The main crystallographic axes X, Y and Z of each SC rod with the spontaneous polarisation $\boldsymbol{P}_s^{(1)}$ are oriented on conditions that X $\parallel OX_1$, Y $\parallel OX_2$ and Z $\parallel \boldsymbol{P}_s^{(1)} \parallel OX_3$. The FC component is used as an inclusion in the polymer matrix that surrounds the system of the aligned SC rods. The shape of each FC inclusion is spheroidal and obeys the equation $(x_1'/a_1)^2 + (x_2'/a_2)^2 + (x_3'/a_3)^2 = 1$ relative to the axes of the rectangular co-ordinate system $(X_1'X_2'X_3')$ rotated by an angle α with respect to $(X_1X_2X_3)$ (inset 1 in Fig. 3.11a). The semi-axes of each FC inclusion are $a_1 = a_2$ and a_3, the aspect ratio of each FC inclusion is $\rho_i = a_1/a_3$, and centres of the inclusions (Fig. 3.11b) occupy sites of a simple tetragonal lattice with unit-cell vectors parallel to the OX_k' axes. We assume that $0 < \rho_i < 1$, and the presence of prolate inclusions facilitates poling of the FC/polymer matrix due to a weaker depolarisation effect in the electric field. The remanent polarisation vector of each FC inclusion is $\boldsymbol{P}_r^{(2)} \uparrow\uparrow OX_3'$, and OX_3' is the poling axis of the matrix (inset 2 in Fig. 3.11a) that represents a composite with 0–3 connectivity in terms of work [7, 13]. The three-component composite shown in Fig. 3.11a is described by 1–0–3 connectivity. It is assumed that the electrodes applied to the composite are perpendicular to the OX_3 axis. By assuming that the linear sizes of the FC inclusions in the 0–3 matrix are significantly smaller than the length of the side of the square being intersected the rod in the (X_1OX_2) plane, we evaluate the effective properties of the 1–0–3 composite in two stages.

At the first stage of averaging, we take into account the electromechanical interaction between the FC inclusions in the 0–3 matrix and evaluate its effective properties by means of the effective field method [7, 10]. An alternative way to find the effective properties of the 0–3 matrix is concerned with the use of the finite element method. COMSOL [44] was applied to obtain the volume-fraction dependence of the effective electromechanical properties of the 0–3 composite within the finite element method framework. The matrix of the effective

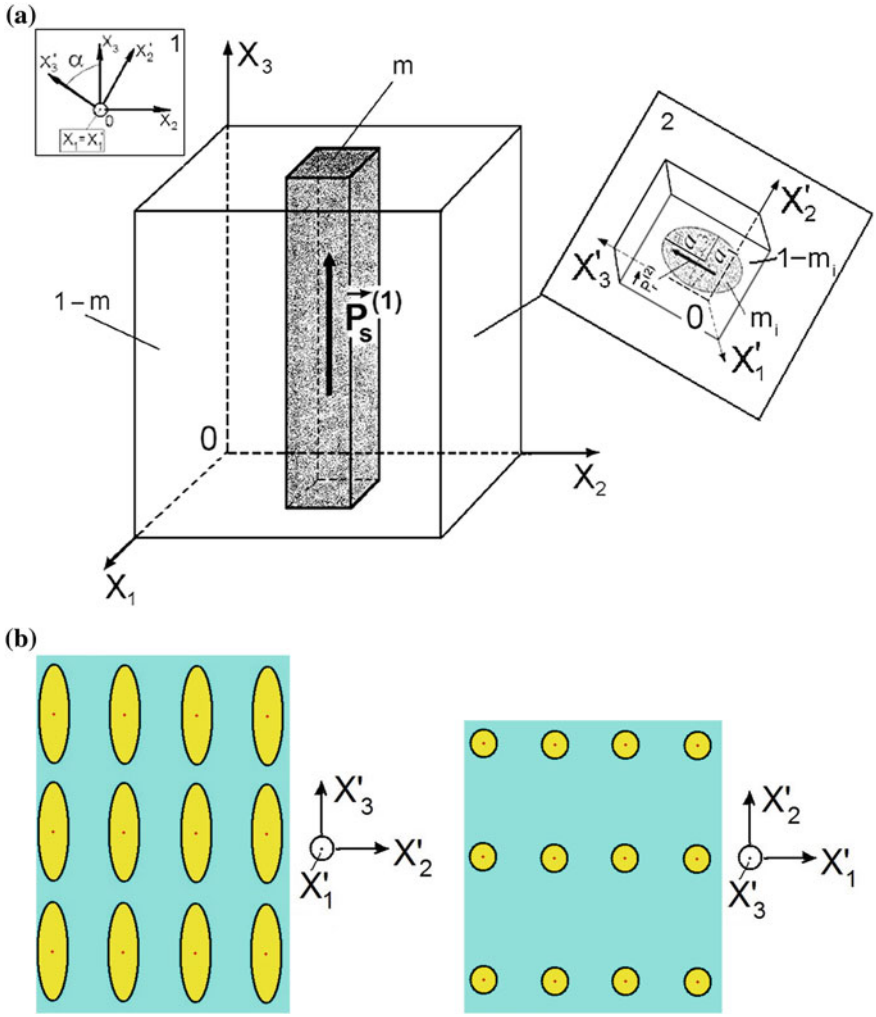

Fig. 3.11 Schematic of the 1–0–3 SC/FC/polymer composite (**a**), and examples of the regular arrangement of spheroidal FC inclusions in the 0–3 matrix along the co-ordinate axes OX_k'. m and $1 - m$ are volume fractions of the SC and surrounding 0–3 matrix, respectively. Rotation of co-ordinate axes $(X_1'X_2'X_3') \rightarrow (X_1X_2X_3)$ is shown in *inset 1*, and the 0–3 matrix is shown in *inset 2*. m_i and $1 - m_i$ are volume fractions of FC and polymer, respectively, in the 0–3 matrix (reprinted from paper by Topolov et al. [44], with permission from Elsevier)

electromechanical properties $\left\|C^*_{0-3}\right\|$ determined using either the effective field method of finite element method represents a function of the volume fraction of FC m_i in the 0–3 composite and the aspect ratio of the FC inclusion ρ_i therein. Taking into account the rotation $(X_1'X_2'X_3') \rightarrow (X_1X_2X_3)$ (see inset 1 in Fig. 3.11a), we find

the matrix of the effective electromechanical properties of the 0–3 composite $\left\|C^*_{0-3}\right\| = \left\|C^*_{0-3}(m_i, \rho_i, \alpha)\right\|$ in the co-ordinate system $(X_1X_2X_3)$.

At the second stage of averaging, the effective electromechanical properties of the 1–0–3 composite with planar interfaces (Fig. 3.11a) are evaluated using the matrix method [7, 10]. The electromechanical properties of the SC rod and 0–3 composite matrix are averaged in the OX_1 and OX_2 directions, in which the periodic structure of the composite is observed. Hereby we take into account electromechanical interactions in a system of 'piezo-active rods—piezo-active matrix'. The effective electromechanical properties of the 1–0–3 composite in the co-ordinate system $(X_1X_2X_3)$ are given by

$$\|C^*\| = \|C^*(m, m_i, \alpha)\| = \begin{pmatrix} \|s^{*E}\| & \|d^*\| \\ \|d^*\| & \|\varepsilon^{*\sigma}\| \end{pmatrix}$$

Among the components of interest for the 1–0–3 composite shown in Fig. 3.11a, we choose the [001]-poled domain-engineered PMN–0.33PT SC, poled $(Pb_{1-x}Ca_x)TiO_3$ FC and araldite. Their properties are shown in Tables 1.1, 2.7 and 3.10. The PMN–0.33PT SC exhibits a high piezoelectric activity and moderate piezoelectric anisotropy (see data from Table 1.1). The $(Pb_{1-x}Ca_x)TiO_3$ FC with $0.20 \le x \le 0.25$ is the second component due to its contrasting properties, compared to PMN–0.33PT SC. As follows from Table 3.10, the FC component exhibits a moderate piezoelectric activity with a large piezoelectric anisotropy. It is known from experimental data [16, 50] that the coercive fields $E_c^{(n)}$ of the PMN–xPT SC ($n = 1$) and $(Pb_{1-x}Ca_x)TiO_3$ FC ($n = 2$) satisfy the condition $E_c^{(1)} \ll E_c^{(2)}$. Such a condition enables initial poling of the 0–3 matrix under a strong electric field with a subsequent poling of the SC rods in the composite (Fig. 3.11a) under a lower electric field.

The piezoelectric properties of the 1–0–3 composite at $\alpha \neq 0°$, $\alpha \neq 180°$ and $0 < m < 1$ are represented by a matrix

$$\|p*\| = \begin{pmatrix} 0 & 0 & 0 & 0 & p^*_{15} & p^*_{16} \\ p^*_{21} & p^*_{22} & p^*_{23} & p^*_{24} & 0 & 0 \\ p^*_{31} & p^*_{32} & p^*_{33} & p^*_{34} & 0 & 0 \end{pmatrix}$$

Table 3.10 Room-temperature elastic compliances s^E_{ab} (in 10^{-12} Pa^{-1}), piezoelectric coefficients d_{fl} (in pC/N) and relative dielectric permittivities $\varepsilon^\sigma_{rr}/\varepsilon_0$ of the poled FC component of the 0–3 matrix

Component	s^E_{11}	s^E_{12}	s^E_{13}	s^E_{33}	s^E_{44}	s_{66}	d_{31}	d_{33}	d_{15}	$\varepsilon^\sigma_{11}/\varepsilon_0$	$\varepsilon^\sigma_{33}/\varepsilon_0$
$(Pb_{0.80}Ca_{0.20}) \cdot TiO_3$ FC [41]	6.04	–1.24	–1.25	6.21	14.7	14.6	–1.33	24.6	26.1	131	135
$(Pb_{0.75}Ca_{0.25}) \cdot TiO_3$ FC [41]	6.00	–1.30	–1.30	6.18	14.8	14.6	–0.364	28.0	28.9	158	163

where $p = d, e, g$, or h. Taking into account the rotation mode (see inset 1 in Fig. 3.11a) and symmetry of the components, we find that the effective properties of the 1–3–0 composite Π^* obey the condition $\Pi^*(m, m_i, \rho_i, \alpha) = \Pi^*(m, m_i, \rho_i, 360° - \alpha)$ [44]. Hereafter we consider examples of the orientation (α) and volume-fraction (m or m_i) dependences of its effective parameters at ρ_i = const.

The orientation dependence of the hydrostatic parameters of the 1–0–3 composite suggests that max g_h^* and max $\left[\left(Q_h^*\right)^2\right]$ are achieved at $\alpha \approx 90°$ and $m_i = 0.12$ (Fig. 3.12). The largest value of g_h^* at $0.1 \le \rho_i \le 0.5$ is related to $m_i \approx 0.12$ and $0.01 < m < 0.03$, and in this m range a local max g_h^* is observed at various values of m_i, ρ_i and α (Fig. 3.12). Our evaluations based on the effective field method (for the 0–3 matrix) and matrix method (for the 1–3–0 composite) lead to absolute max $d_h^* = 305$ pC/N at $m = 0.532$, $m_i = 0.12$, $\rho_i = 0.1$, and $\alpha = 90°$ [44].

Using the matrix method, we find for the related 1–3 PMN–0.33PT SC/araldite composite (i.e., in a case of $m_i = 0$ in Fig. 3.11a), that absolute max $g_h^* = 158$ mV m/N, max $\left[\left(Q_h^*\right)^2\right] = 8.27 \cdot 10^{-12}$ Pa^{-1} and max $d_h^* = 274$ pC/N are achieved at $m = 0.016$, 0.103 and 0.509, respectively. At $m = 0.05$ for the 1–3 PMN–0.33PT SC/araldite composite, we find $g_h^* = 115$ mV m/N, and this value is considerably smaller than g_h^* near the maxima in Fig. 3.12a. The large values of $\left(Q_h^*\right)^2$ (Fig. 3.12b) and d_h^* in the 1–0–3 composite are due to the presence of the 0–3 matrix that comprises of a FC component with piezoelectric coefficients $d_{3f}^{(2)}$ that obey the condition [41] $d_{33}^{(2)} / \left|d_{31}^{(2)}\right| \gg 1$. At the rotation angle $\alpha = 90°$, the remanent polarisation vector $\boldsymbol{P}_r^{(2)}$ of each FC inclusion (see inset 2 in Fig. 3.11a) is parallel to OX_2, and this $\boldsymbol{P}_r^{(2)}$ orientation leads to a decrease in $\left|d_{32}^*\right|$ with minor changes in d_{31}^* and d_{33}^* (or g_{31}^* and g_{33}^*, respectively) as a result of the weak lateral piezoelectric effect in the 0–3 FC/polymer matrix. As a consequence of the reduced $\left|d_{32}^*\right|$, we observe an increase in both d_h^* and g_h^* of the 1–3–0 composite.

We note that the elastic anisotropy of the 0–3 matrix with highly prolate FC inclusions is an additional factor in increasing the hydrostatic parameters of the 1–0–3 composite. For instance, ratios of the elastic compliances of a 0–3 $(Pb_{0.75}Ca_{0.25})TiO_3$ FC/araldite composite with spheroidal inclusions (see Fig. 3.11b) are $s_{11,0-3}^E / s_{12,0-3}^E = -2.21$, $s_{11,0-3}^E / s_{13,0-3}^E = -6.52$ and $s_{11,0-3}^E / s_{33,0-3}^E = 1.95$ at $\rho_i = 0.1$ and $m_i = 0.10$. At $\rho_i = 0.3$ and $m_i = 0.10$, for the same composite we find $s_{11,0-3}^E / s_{12,0-3}^E = -2.52$, $s_{11,0-3}^E / s_{13,0-3}^E = -3.51$ and $s_{11,0-3}^E / s_{33,0-3}^E = 1.25$. It is seen that a significant decrease of $\left|s_{11,0-3}^E / s_{13,0-3}^E\right|$ and $\left|s_{11,0-3}^E / s_{33,0-3}^E\right|$ takes place when the piezoelectric activity decreases. This orientation effect in the 1–0–3 composite favours an increase in $\left(Q_h^*\right)^2$ and d_h^* near its maxima by approximately 29 and 11 %, respectively [44], in comparison to the aforementioned 1–3 PMN–0.33PT SC/araldite composite. The studied 1–0–3

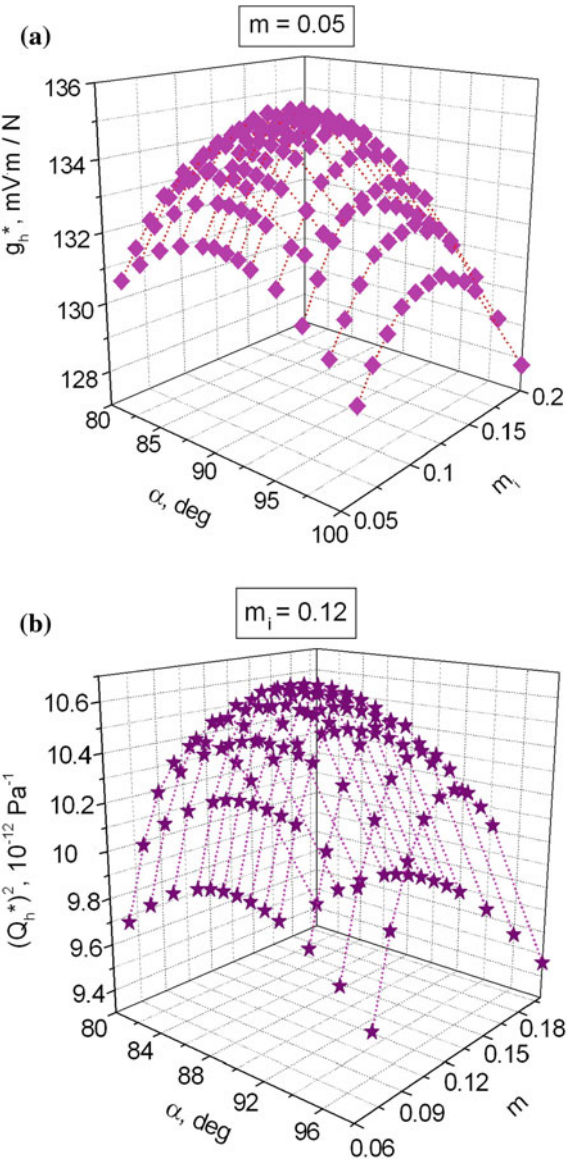

Fig. 3.12 Examples of the orientation dependence of the hydrostatic parameters of the 1–0–3 PMN–0.33PT SC/$(Pb_{0.75}Ca_{0.25})TiO_3$ FC/araldite composite at $\rho_i = 0.1$: (**a**) near local $\max g_h^*(0.05, m_i, 0.1, \alpha)$ and (**b**) near absolute $\max\left\{\left[Q_h^*(m, 0.12, 0.1, \alpha)\right]^2\right\}$. Electromechanical properties of the 0–3 matrix at the first stage of averaging were determined by means of the effective field method (reprinted from paper by Topolov et al. [44], with permission from Elsevier)

composite is also attractive due to large values of local maxima of d_h^*, g_h^* and $\left(Q_h^*\right)^2$ at volume fractions of FC inclusions m_i = const, especially at $m_i < 0.15$.

Replacing the $(Pb_{0.75}Ca_{0.25})TiO_3$ FC with $(Pb_{1-x}Ca_x)TiO_3$ at $x = 0.20$–0.24 leads to changes in the hydrostatic parameters of the 1–0–3 composite by 1–3 % at fixed values of m, m_i and ρ_i. The $(Pb_{1-x}Ca_x)TiO_3$ FCs at $x = 0.20$–0.24 are characterised by the large piezoelectric anisotropy: e.g., $d_{33}^{(2)}/\left|d_{31}^{(2)}\right|$ = 18.7, 30.3 and 39.8 at

x = 0.20, 0.23 and 0.24, respectively [41]. These FCs exhibit an appreciable elastic anisotropy that is typical of modified $PbTiO_3$ FCs [50]. Our results suggest that the large piezoelectric anisotropy of the $(Pb_{1-x}Ca_x)TiO_3$ FC leads to a large piezoelectric anisotropy of the 0–3 composite and favours the orientation effect in the 1–0–3 composite and improving their hydrostatic parameters in comparison to the 1–3 composite.

3.5.2 New Aspect-Ratio Effect

In Sect. 3.5.2 we discuss an influence of the aspect ratio of FC inclusions ρ_i in the 0–3 matrix (see inset 2 in Fig. 3.11a) on the piezoelectric performance and hydrostatic parameters of the 1–0–3 composite. In our study, the [001]-poled domain-engineered PMN–0.33PT SC is regarded as the main piezoelectric component (see the full set of its electromechanical constants in Table 1.1), the modified $PbTiO_3$ FC is the main component in the 0–3 matrix (see the full set of electromechanical constants of the modified $PbTiO_3$ (I) FC in Table 1.2), and the polymer component is either araldite or polyurethane (their properties are shown in Table 2.7). It is obvious that the SC and FC components are selected due to their contrasting electromechanical properties.

An important example of the dependence of the piezoelectric coefficients g_{33}^* and g_h^* and squared figures of merit $\left(Q_{3j}^*\right)^2$ on the aspect ratio ρ_i is shown in Fig. 3.13. Distinct changes in the effective parameters of the 1–0–3 composite are observed [45] at

$$0.01 < \rho_i < 2. \tag{3.12}$$

The shape of the FC inclusion in the aspect-ratio range (3.12) changes from highly prolate ($\rho_i << 1$) to oblate ($\rho_i > 1$). These changes in the microgeometry of the 0–3 matrix give rise to significant changes in its elastic properties and ratios of elastic compliances of the matrix $s_{1b}^{(m),E}/s_{kl}^{(m),E}$ which have a strong influence on the piezoelectric properties and their anisotropy in the 1–0–3 composite as a whole. We add that some examples of the influence of the elastic anisotropy of the 0–3 matrix on the performance of the 1–0–3 composite were considered in Sect. 3.5.1.

Now we compare some effective parameters which are calculated using different methods [45]. In the first case we calculate the effective properties of the 0–3 matrix by means of the finite element method and then the effective properties of the 1–0–3 composite as a whole by means of the matrix method. In the second case we apply the effective field method to evaluate the effective properties of the 0–3 matrix and the matrix method to find the effective properties of the 1–0–3 composite. Example results are given for comparison in Table 3.11. As follows from Table 3.11, the effective parameters concerned with the longitudinal [g_{33}^* and $\left(Q_{33}^*\right)^2$], lateral

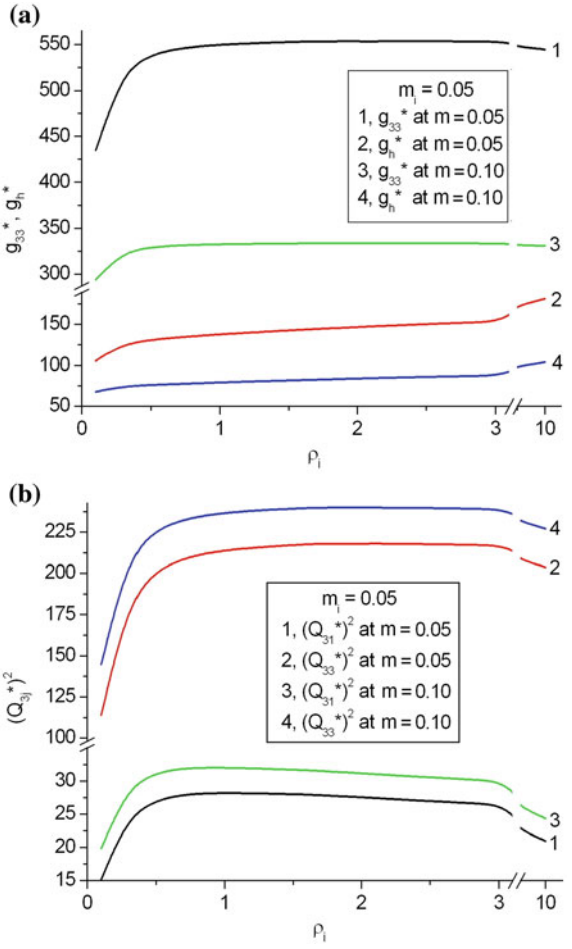

Fig. 3.13 Aspect-ratio dependence of the piezoelectric coefficient g_{33}^* and hydrostatic piezoelectric coefficient g_h^* (**a** in mV m/N), and squared figures of merit $\left(Q_{3j}^*\right)^2$ (**b** in 10^{-12} Pa^{-1}) of the 1–0–3 PMN–0.33PT SC/modified $PbTiO_3$ FC/polyurethane composite at volume fractions m_i = const (FC inclusions in the 0–3 matrix) and m = const (SC rods in the composite), see the schematic in Fig. 3.11a. At the first stage of averaging, electromechanical properties of the 0–3 matrix were evaluated by means oft he effective field method (reprinted from paper by Topolov et al. [45], with permission from Elsevier)

$\left[\left(Q_{31}^*\right)^2\right]$ and hydrostatic $\left[\left(Q_h^*\right)^2\right]$ piezoelectric effects of the 1–0–3 composite are in agreement. The largest relative error (δ = 10–11 %) is related to squared figures of merit $\left(Q_{3j}^*\right)^2$ and $\left(Q_h^*\right)^2$. These parameters combine the piezoelectric activity and sensitivity. Maxima of $\left(Q_{3j}^*\right)^2$ and $\left(Q_h^*\right)^2$ are observed at relatively small volume fractions m of SC (approximately 0.1) due to a non-monotonic behaviour of g_{3j}^* and g_h^*, respectively. The location of max g_{33}^*, min g_{31}^* and max g_h^* at $m << 1$ (as a rule, less than 0.05) strongly depends on the elastic and dielectric properties of the 0–3 matrix. It is seen that differences between the parameters calculated for the 1–0–3 composite using different methods are located near maxima of $\left(Q_{3j}^*\right)^2$ and $\left(Q_h^*\right)^2$, i.e., at m = 0.05 or 0.10 (Table 3.11).

Table 3.11 Comparison of effective parameters calculated for the 1–0–3 PMN–0.33PT SC/modified $PbTiO_3$ FC/polymer composite using either the finite element method $\left(\Pi^*_{FEM}\right)$ or effective field method $\left(\Pi^*_{EFM}\right)$ to evaluate properties of the 0–3 matrix

Evaluation method for 0–3 matrix properties	ρ_i	m_i	m	g^*_{33}, mV m/N	$\left(Q^*_{33}\right)^2$, 10^{-12} Pa^{-1}	$\left(Q^*_{31}\right)^2$, 10^{-12} Pa^{-1}	$\left(Q^*_h\right)^2$, 10^{-12} Pa^{-1}
1–0–3 PMN–0.33PT SC/modified $PbTiO_3$ FC/araldite composite							
Finite element method	1.5	0.05	0.05	433	96.6	12.3	7.03
	2.0	0.05	0.05	433	96.4	12.1	7.30
	2.5	0.05	0.05	432	95.7	11.8	7.57
	1.5	0.10	0.05	406	81.3	9.84	6.75
	2.0	0.10	0.05	405	80.6	9.45	7,22
	2.5	0.10	0.05	403	79.2	8.98	7.65
	1.5	0.05	0.10	291	126	16.6	8.27
	2.0	0.05	0.10	291	126	16.3	8.58
	2.5	0.05	0.10	291	125	15.9	8.90
	1.5	0.10	0.10	281	110	13.8	8,21
	2.0	0.10	0.10	281	109	13.3	8.77
	2.5	0.10	0.10	280	108	12.7	9.30
Effective field method	1.5	0.05	0.05	438	98.8	12.4	7.39
	2.0	0.05	0.05	439	99.2	12.2	7.77
	2.5	0.05	0.05	439	99.1	12.0	8.06
	1.5	0.10	0.05	418	86.8	10.4	7.33
	2.0	0.10	0.05	420	87.5	10.2	7.97
	2.5	0.10	0.05	420	87.5	9.88	8.50
	1.5	0.05	0.10	293	128	16.6	8.61
	2.0	0.05	0.10	293	128	16.4	9.04
	2.5	0.05	0.10	293	128	16.1	9.37
	1.5	0.10	0.10	285	115	14.4	8.47
	2.0	0.10	0.10	286	116	14.0	9.48
	2.5	0.10	0.10	286	116	13.6	10.1
1–0–3 PMN–0.33PT SC/modified $PbTiO_3$ FC/polyurethane composite							
Finite element method	1.5	0.05	0.05	549	212	27.7	13.8
	2.0	0.05	0.05	549	212	27.2	14.4
	2.5	0.05	0.05	548	210	26.5	15.0
	1.5	0.10	0.05	525	182	22.6	13.7
	2.0	0.10	0.05	524	180	21.6	14.8
	2.5	0.10	0.05	522	177	20.4	15.8
	1.5	0.05	0.10	332	235	31.5	13.8
	2.0	0.05	0.10	332	235	30.9	14.4
	2.5	0.05	0.10	332	233	30.2	15.0
	1.5	0.10	0.10	325	209	26.7	14.2
	2.0	0.10	0.10	324	207	25.6	15.2
	2.5	0.10	0.10	324	204	24.4	16.3

(continued)

Table 3.11 (continued)

Evaluation method for 0–3 matrix properties	ρ_i	m_i	m	g_{33}^*, mV m/N	$\left(Q_{33}^*\right)^2$, 10^{-12} Pa^{-1}	$\left(Q_{31}^*\right)^2$, 10^{-12} Pa^{-1}	$\left(Q_h^*\right)^2$, 10^{-12} Pa^{-1}
Effective field method	1.5	0.05	0.05	553	217	28.1	14.4
	2.0	0.05	0.05	553	218	27.5	15.3
	2.5	0.05	0.05	553	218	27.0	16.1
	1.5	0.10	0.05	531	194	23.7	14.8
	2.0	0.10	0.05	536	195	23.0	16.3
	2.5	0.10	0.05	536	195	22.2	17.5
	1.5	0.05	0.10	333	240	31.8	14.4
	2.0	0.05	0.10	334	240	31.2	15.2
	2.5	0.05	0.10	334	240	30.6	16.0
	1.5	0.10	0.10	328	219	27.7	15.1
	2.0	0.10	0.10	328	220	26.8	16.6
	2.5	0.10	0.10	328	220	26.0	17.8

Replacing araldite with a more compliant polyurethane (their elastic properties are shown in Table 2.7) in the 0–3 matrix leads to an increase of all of the aforementioned effective parameters of the 1–0–3 composite (see Table 3.11). Such an effect is due to the more pronounced longitudinal and hydrostatic piezoelectric effects in a 1–3-type composite [7] that contains a more compliant matrix which allows a larger free deformation of the embedded piezoelectric rods. The use of a more compliant matrix has a significant influence on the piezoelectric response of the 1–0–3 composite along different co-ordinate axes.

Table 3.11 suggests that the relation

$$\left(Q_{33}^*\right)^2/\left(Q_{31}^*\right)^2 \approx 8-9 \tag{3.13}$$

holds at various values of m, m_i and ρ_i. A relatively large $\left(Q_{33}^*\right)^2/\left(Q_{31}^*\right)^2$ ratio is achieved due to the effect of the elastic properties of the 0–3 matrix on the lateral piezoelectric response. The oblate FC inclusions in this matrix can weaken the piezoelectric coefficient d_{31}^* of the 1–0–3 composite due to the aforementioned elastic anisotropy of the 0–3 matrix (see Sect. 3.5.1).

Of particular interest is a case of a piezo-passive 0–3 matrix to examine the influence of the FC inclusion elastic properties on the composite performance. Now it is assumed that the FC inclusions in a polymer medium (inset 2 in Fig. 3.11a) have not been poled and, therefore, remain piezo-passive and isotropic. By varying the aspect ratio ρ_i of these inclusions it is possible to observe changes in the effective parameters of the 1–0–3 composite (Table 3.12), however these parameters become larger than those in the case of the poled (piezo-active) 0–3 FC/polymer matrix. This is a result of a decrease in the dielectric permittivity of the piezo-passive 0–3 matrix that leads to an appreciable decrease of $\varepsilon_{33}^{*\sigma}$ of the 1–0–3

Table 3.12 Effective parameters calculated for the 1–0–3 PMN–0.33PT SC/modified $PbTiO_3$ FC/polyurethane composite in a case of a piezo-passive 0–3 matrix[a] (reprinted from paper by Topolov et al. [45], with permission from Elsevier)

ρ_i	m_i	m	g_{33}^*, mV m/N	$\left(Q_{33}^*\right)^2$, 10^{-12} Pa^{-1}	$\left(Q_{31}^*\right)^2$, 10^{-12} Pa^{-1}	d_h^*, pC/N	g_h^*, mV m/N	$\left(Q_h^*\right)^2$, 10^{-12} Pa^{-1}
1.5	0.05	0.05	553	218	28.1	102	143	14.5
2.0	0.05	0.05	554	218	27.5	105	147	15.4
2.5	0.05	0.05	554	218	27.0	107	150	16.1
1.5	0.10	0.05	535	194	23.7	101	148	14.9
2.0	0.10	0.05	536	185	23.0	105	155	16.3
2.5	0.10	0.05	536	195	22.2	109	161	17.6
1.5	0.05	0.10	333	240	31.7	177	81.9	14.5
2.0	0.05	0.10	334	240	31.2	182	84.1	15.3
2.5	0.05	0.10	334	240	30.6	186	86.1	16.0
1.5	0.10	0.10	328	220	27.7	176	86.2	15.2
2.0	0.10	0.10	328	221	26.8	195	90.2	16.6
2.5	0.10	0.10	328	220	25.9	191	93.5	17.9

[a]Electromechanical properties of the 0–3 matrix were evaluated by means of the effective field method

composite at relatively small SC volume fractions. Results given in Table 3.12 suggest that the role of the elastic anisotropy in achieving high piezoelectric performance for the 1–0–3 composite remains dominant irrespective of the piezoelectric activity of its 0–3 matrix. Thus, during the manufacture of the 1–0–3 composite shown in Fig. 3.11a, there is no need to pole the 0–3 matrix under a relatively high electric field, as applied, for instance, to the $PbTiO_3$-type FC composite systems [50]. An incompleteness of the poling of the 0–3 matrix is avoided by this way, and a smaller dielectric permittivity $\varepsilon_{33}^{*\sigma}$ in the 1–0–3 composite favours its higher piezoelectric sensitivity.

The performance of the 1–0–3 composite is compared to data [51] on a 1–0–3 FC/FC/polyurethane composite where the highly piezo-active PCR-7M FC (a PZT-type composition, see data in Table 1.2) is the main component. Parameters that characterise the piezoelectric sensitivity of the 1–0–3 PCR-7M FC/PCR-7M FC/polyurethane composite are $g_{33}^* \approx 400$ mV m/N, $g_h^* \approx 200$ mV m/N, and the hydrostatic piezoelectric activity is characterized by $d_h^* \approx 350$ pC/N [51]. These effective parameters are comparable to those related to the 1–0–3 relaxor-ferroelectric SC/FC/polyurethane composite [45] that consists of contrasting components. The maximum value of g_{33}^* determined for a 1–3 PMN–0.30PT/epoxy composite [19] is 440 mV m/N (at the volume fraction of SC $m = 0.018$) and is comparable to values of g_{33}^* from Tables 3.11 and 3.12. A 1–3 composite based on PMN–PT SC is characterised by $d_h^* = 111$ pC/N, $g_h^* = 37$ mV m/N and $\left(Q_h^*\right)^2 = 4.12 \cdot 10^{-12}$ Pa^{-1} [52], and these parameters are smaller than those given in Tables 3.11 and 3.12. It should be added that the $\left(Q_h^*\right)^2$ values shown in Tables 3.11

and 3.12 are about 1.5–3 times more than $\left(Q_h^*\right)^2$ related to conventional 1–3 FC/polymer composites [7, 8, 13–15].

The next example of high-performance composite systems is related to the 1–0–3 composite based on the [001]-poled PZN–0.08PT SC [46]. This SC if of specific interest because of a high piezoelectric activity (for example, the longitudinal piezoelectric coefficient $d_{33}^{(1)}$ = 2890 pC/N, see Table 1.1) and small negative hydrostatic piezoelectric coefficients $d_h^{(1)}$ = –20 pC/N and $g_h^{(1)}$ = –0.293 mV m/N. It is now assumed that the 0–3 matrix surrounding the SC rods (Fig. 3.11a) contains modified $PbTiO_3$ FC inclusions in a polymer medium. The electromechanical properties of the 0–3 matrix wherein a regular arrangement of the spheroidal FC inclusions is assumed (Fig. 3.11b), are evaluated using either the finite element method or effective field method, and the subsequent averaging procedure for the system 'rods—matrix' is carried out using the matrix method. Results of our calculations of squared figures of merit and related parameters of the PZN–0.08PT-based composite are shown in Tables 3.13 and 3.14.

Data from Tables 3.13 and 3.14 show the active role of the matrix subsystem in achieving large piezoelectric coefficients and figures of merit of the 1–0–3 composite. Even at relatively small volume fractions of the FC inclusions m_i in the 0–3 matrix, changes in the aspect ratio ρ_i lead to changes in the aforementioned parameters of the 1–0–3 composite. We see that these changes take place irrespective of the piezoelectric activity of the 0–3 matrix. In general, a good correlation between the effective parameters calculated using different methods (see Tables 3.13 and 3.14) is observed. The smaller dielectric permittivity $\varepsilon_{33}^{*\sigma}$ (due to the lack of the piezoelectric contribution into the dielectric permittivity of the 0–3 matrix $\varepsilon_{33}^{(m)}$) favours a higher piezoelectric sensitivity of the 1–0–3 composite in accordance with the relation [11, 12] $g_{3j}^* = d_{3j}^*/\varepsilon_{33}^{*\sigma}$ (j = 1, 2 and 3). This leads to an increase in $\left(Q_{3j}^*\right)^2$ and $\left(Q_h^*\right)^2$ (Table 3.14) in comparison to those (Table 3.13) related to the composite with a piezo-active 0–3 matrix. Moreover, the elastic properties of the polymer component and, therefore, the 0–3 matrix strongly influences the studied parameters of the 1–0–3 composite: we see the larger values of $\left(Q_{3j}^*\right)^2$ and $\left(Q_h^*\right)^2$ in the presence of the softer, polyurethane, component.

We add for comparison, that at m_i = 0 (i.e., for the 1–3 PZN–0.08PT SC/polyurethane composite), absolute maxima are achieved as follows [46]: max d_h^* = 254 pC/N (at the volume fraction of SC m = 0.341), max g_h^* = 145 mV m/N (at m = 0.012) and max $\left[\left(Q_h^*\right)^2\right]$ = 9.53 · 10^{-12} Pa^{-12} (at m = 0.088). These values are considerably less than those given in Tables 3.13 and 3.14. Our comparison of data from Tables 3.12 and 3.14 suggests that in the 1–0–3 PZN–0.08PT SC/modified $PbTiO_3$ FC/polyurethane composite, larger values of its squared figures of merit

Table 3.13 Effective parameters calculated for the 1–0–3 PZN–0.08PT SC/modified $PbTiO_3$ FC/polymer composite in a case of a piezo-active 0–3 matrix[a]

ρ_i	m_i	m	g_{33}^*, mV m/N	$(Q_{33}^*)^2$, 10^{-12} Pa^{-1}	$(Q_{31}^*)^2$, 10^{-12} Pa^{-1}	d_h^*, pC/N	g_h^*, mV m/N	$(Q_h^*)^2$, 10^{-12} Pa^{-1}
1–0–3 PZN–0.08PT SC/modified $PbTiO_3$ FC/araldite composite								
1.5	0.05	0.05	287	56.1	5.68	71.2	104	7.43
2.0	0.05	0.05	286	56.0	5.68	70.9	104	7.37
2.5	0.05	0.05	285	55.5	5.69	70.0	103	7.18
1.5	0.10	0.05	264	46.5	5.75	52.2	78.1	4.08
2.0	0.10	0.05	263	46.0	5.77	51.0	76.6	3.91
2.5	0.10	0.05	261	45.1	5.78	49.1	74.0	3.63
1.5	0.05	0.10	224	85.9	9.39	130	75.9	9.86
2.0	0.05	0.10	224	85.7	9.39	129	75.6	9.78
2.5	0.05	0.10	223	85.1	9.41	128	74.8	9.55
1.5	0.10	0.10	212	73.5	9.63	95.9	58.4	5.60
2.0	0.10	0.10	211	72.8	9.65	93.8	57.3	5.37
2.5	0.10	0.10	210	71.5	9.67	90.3	55.5	5.01
1–0–3 PZN–0.08PT SC/modified $PbTiO_3$ FC/polyurethane composite								
1.5	0.05	0.05	411	139	5.23	208	252	52.2
2.0	0.05	0.05	410	139	5.23	207	251	51.9
2.5	0.05	0.05	409	137	5.23	205	249	51.1
1.5	0.10	0.05	384	117	5.30	175	220	38.6
2.0	0.10	0.05	382	115	5.30	173	218	37.7
2.5	0.10	0.05	379	113	5.31	169	215	36.3
1.5	0.05	0.10	285	179	8.35	357	162	57.8
2.0	0.05	0.10	284	179	8.36	355	161	57.5
2.5	0.05	0.10	284	177	8.36	353	161	56.7
1.5	0.10	0.10	273	156	8.52	305	145	44.3
2.0	0.10	0.10	272	155	8.53	301	144	43.4
2.5	0.10	0.10	271	152	8.55	295	142	42.0

[a]Electromechanical properties of the 0–3 matrix were evaluated by means of the finite element method [46]

$(Q_{33}^*)^2$, $(Q_{31}^*)^2$ and $(Q_h^*)^2$ are achieved due to the more pronounced piezoelectric anisotropy that is also caused by the elastic properties of the 0–3 matrix. The system of oblate FC inclusions in the softer polymer matrix leads to a large decrease of the transversal piezoelectric response of the composite. As a consequence, irrespective of the piezoelectric activity of the 0–3 matrix, the condition (3.8) holds for the 1–0–3 PZN–0.08PT SC/modified $PbTiO_3$ FC/polyurethane composite (see data in Tables 3.13 and 3.14). The validity of the condition (3.8) and the large values of the squared figures of merit $(Q_{33}^*)^2$, $(Q_{31}^*)^2$ and $(Q_h^*)^2$ are to be taken into account for energy-harvesting applications of the studied 1–0–3 composite.

Table 3.14 Effective parameters calculated for the 1–0–3 PZN–0.08PT SC/modified $PbTiO_3$ FC/polymer composite in a case of a piezo-passive 0–3 matrix[a]

ρ_i	m_i	m	g_{33}^*, mV m/N	$(Q_{33}^*)^2$, 10^{-12} Pa^{-1}	$(Q_{31}^*)^2$, 10^{-12} Pa^{-1}	d_h^*, pC/N	g_h^*, mV m/N	$(Q_h^*)^2$, 10^{-12} Pa^{-1}
1–0–3 PZN–0.08PT SC/modified $PbTiO_3$ FC/araldite composite								
1.5	0.05	0.05	288	56.9	5.66	72.9	107	7.77
2.0	0.05	0.05	289	57.2	5.66	73.4	107	7.87
2.5	0.05	0.05	289	57.1	5.66	73.3	107	7.85
1.5	0.10	0.05	270	49.2	5.70	58.0	86.3	5.01
2.0	0.10	0.05	271	49.6	5.70	58.9	87.6	5.16
2.5	0.10	0.05	272	49.6	5.70	58.9	87.7	5.16
1.5	0.05	0.10	225	87.0	9.35	133	77.5	10.3
2.0	0.05	0.10	225	87.3	9.34	134	77.9	10.4
2.5	0.05	0.10	225	87.2	9.34	134	77.9	10.4
1.5	0.10	0.10	215	77.1	9.51	107	64.2	6.85
2.0	0.10	0.10	216	77.7	9.85	108	65.1	7.05
2.5	0.10	0.10	216	77.7	9.49	108	65.1	7.04
1–0–3 PZN–0.08PT SC/modified $PbTiO_3$ FC/polyurethane composite								
1.5	0.05	0.05	413	141	5.19	211	255	53.6
2.0	0.05	0.05	414	141	5.18	211	255	53.8
2.5	0.05	0.05	413	141	5.18	211	256	53.8
1.5	0.10	0.05	392	124	5.21	186	231	42.9
2.0	0.10	0.05	393	124	5.20	187	232	43.5
2.5	0.10	0.05	393	124	5.20	187	232	43.3
1.5	0.05	0.10	286	181	8.28	363	163	59.3
2.0	0.05	0.10	286	181	8.27	363	164	59.5
2.5	0.05	0.10	286	181	8.27	363	164	59.4
1.5	0.10	0.10	277	163	8.36	323	151	48.9
2.0	0.10	0.10	277	164	8.34	325	152	49.4
2.5	0.10	0.10	277	164	8.34	324	152	49.3

[a]Electromechanical properties of the 0–3 matrix were evaluated by means of the effective field method [7] at neglecting a piezoelectric activity of FC

3.6 Three Figures of Merit for Transmitter-Receiver or Pulse-Echo Systems

In Sect. 2.6.2 we discussed ECFs and their anisotropy in 1–3–0 composites based on relaxor-ferroelectric SCs. Now we consider a system of squared figures of merit [6, 53] of the 1–3–0 composite as follows:

$$\left(Q_{33}^*\right)^2 = d_{33}^* g_{33}^*, F_{q,33}^* = \left(d_{33}^*\right)^2 \text{ and } F_{E,33}^* = \left(k_{33}^*\right)^4 / \left(Z_{a,33}^*\right)^2 \tag{3.14}$$

for the longitudinal piezoelectric effect (33 oscillation mode), and

$$\left(Q_{3j}^{*}\right)^{2} = d_{3j}^{*} g_{3j}^{*}, F_{q,3j}^{*} = \left(d_{3j}^{*}\right)^{2} \text{ and } F_{E,3j}^{*} = \left(k_{3j}^{*}\right)^{4} / \left(Z_{a,jj}^{*}\right)^{2} \tag{3.15}$$

for the transversal piezoelectric effect (31 and 32 oscillation modes, j = 1 and 2). The squared figures of merit from (3.14) and (3.15) are used to characterise a performance of the piezoelectric transmitter-receiver or pulse-echo system. In (3.14) and (3.15), $Z_{a,ff}^{*} = \rho^{*} v_{f}^{*}$ is the specific acoustic impedance on either the polar (f = 3) or non-polar (f = 1 or 2) direction, ρ^{*} is the density of the composite, and v_{f}^{*} is the sound velocity along the co-ordinate axis OX_f.

We analyse the squared figures of merit from (3.14) and (3.15) for the 1–3–0 SC/porous polymer composite described in Sect. 2.6.2. Both the SC rods in the form of a rectangular parallelepiped with a square base and spheroidal air pores in the polymer matrix are distributed regularly. The main component of the 1–3–0 composite is the [001]-poled PMN–0.33PT SC with a high piezoelectric activity (see electromechanical constants in Table 1.1), and the SC rods are surrounded by a piezo-passive porous polyurethane matrix with 3–0 connectivity. Data on the squared figures of merit are shown in Table 3.15 and Fig. 3.14. It is seen that the studied 1–3–0 composite with the system of highly oblate spheroidal air pores in the polymer medium (i.e., at the aspect ratio $\rho_p >> 1$) provides the best set of the parameters from (3.14) and (3.15). The highly oblate pores strongly influence the anisotropy of the elastic properties of the matrix and the piezoelectric response of the composite as a whole: with increasing ρ_p, the transversal piezoelectric effect weakens. As a consequence, conditions

$$\left(Q_{33}^{*}\right)^{2} \gg \left(Q_{31}^{*}\right)^{2} \text{ and } F_{E,33}^{*} \gg F_{E,31}^{*} \tag{3.16}$$

are valid in wide ranges of m, m_p and ρ_p.

Maxima of some squared figures of merit at $\rho_p >> 1$ are achieved at relatively small volume fractions of SC m (see Table 3.15 and curve 4 in Fig. 3.14b). However changes in values of the squared figures of merit with increasing m are not considerable (see Fig. 3.14b), and it would be reasonable to manufacture a high-performance composite sample at m = 0.05–0.10. In this volume-fraction range of SC, the influence of the porous polymer matrix on the performance of the composite is still significant. Graphs in Fig. 3.14 contain curves 1 related to the 1–3 composite with the monolithic polymer matrix. It is seen that the squared figures of merit of the 1–3 composite are considerably less than those of the studied 1–3–0 composite, and this effect is caused by the matrix. Thus, the porous polymer matrix improves the set of effective parameters of the 1–3–0 composite that are suitable for piezoelectric transmitter-receiver and/or pulse-echo systems where the 33 oscillation mode is dominant.

Table 3.15 Maximum values of squared figures of merit from (3.14) and (3.15) and related volume fractions of SC m in the 1–3–0 PMN–0.33PT SC/porous polyurethane composite

ρ_p	max $\left(Q^*_{33}\right)^2$, 10^{-10} Pa^{-1}	max $F^*_{E,33}$, 10^{-14} Rayl^{-2}	max $\left(Q^*_{31}\right)^2$, 10^{-11} Pa^{-1}	max $F^*_{E,31}$, 10^{-15} Rayl^{-2}
Composite at $m_p = 0.1$				
1	2.86 (m = 0.088)	12.8 (m = 0.073)	3.74 (m = 0.106)	2.07 (m = 0.077)
10	4.18 (m = 0.056)	20.8 (m = 0.053)	2.50 (m = 0.077)	1.03 (m = 0.054)
100	15.2 (m = 0.014)	91.1 (m = 0.019)	0.446 (m = 0.016)	0.0389 (m = 0.014)
Composite at $m_p = 0.2$				
1	3.44 (m = 0.070)	17.6 (m = 0.060)	4.20 (m = 0.080)	2.48 (m = 0.060)
10	6.36 (m = 0.035)	37.8 (m = 0.037)	2.21 (m = 0.041)	0.847 (m = 0.032)
100	29.4 (m = 0.008)	204 (m = 0.010)	0.267 (m = 0.007)	0.0143 (m = 0.007)

Notes

1. $F^*_{q,33}$ and $F^*_{q,31}$ are monotonically increasing functions of the volume fraction of SC m irrespective of the parameters m_p and ρ_p of the porous matrix
2. Volume fractions m related to maximum values of the effective parameters in the 2nd–5th columns are given in parentheses
3. The [001]-poled PMN–0.33PT SC is characterised by $(Q^{(1)}_{33})^2 = 1.10 \cdot 10^{-10}$ Pa^{-1}, $F^{(1)}_{q,33} = 7.95 \cdot 10^{-18}$ C^2/N^2, $F^{(1)}_{E,33} = 1.25 \cdot 10^{-14}$ Rayl^{-2}, $(Q^{(1)}_{31})^2 = 0.244 \cdot 10^{-10}$ Pa^{-1}, $F^{(1)}_{q,31} = 1.76 \cdot 10^{-18}$ C^2/N^2, and $F^{(1)}_{E,31} = 0.106 \cdot 10^{-14}$ Rayl^{-2}. The listed parameters were calculated using experimental data from work [16]

3.7 Related Parameters

Now we consider effective parameters that can be regarded as 'relatives' to the figures of merit. If the piezo-composite element radiates acoustic waves, then its specific acoustic power at low frequencies is proportional to $\left(d^*_{ik}/v^{*E}_k\right)^2 E^2$ [54], where d^*_{ik} is the piezoelectric coefficient, $v^{*E}_k = \left(\rho^* s^{*E}_{kk}\right)^{-1/2}$ is the sound velocity measured along OX_k, E is electric field applied to the element and ρ^* is its effective density. It is assumed that frequencies are much less than the resonance frequency of the piezoelectric element. A ratio of the specific acoustic powers related to the longitudinal and transversal piezoelectric responses of the element is given by

$$r^*_{pow} = \left(d^*_{33}/v^{*E}_3\right)^2 / \left(d^*_{31}/v^{*E}_1\right)^2 = \left(\zeta^*_{d3j}\right)^2 s^{*E}_{33}/s^{*E}_{11} \tag{3.17}$$

In (3.17), ζ_{d3j}* is the anisotropy factor concerned with the piezoelectric coefficients d^*_{3j} [see (2.4)], and s^{*E}_{ab} is the elastic compliance at E = const.

Oscillations of the piezoelectric element in the form of the rectangular parallelepiped elongated on the OX_3 direction and conversion of energy in the piezoelectric element can be characterised by coefficients of electromechanical transformation N^*_{33} and N^*_{31} [54, 55] at the longitudinal and transversal oscillation modes, respectively. According to work [54], these coefficients linearly depend on

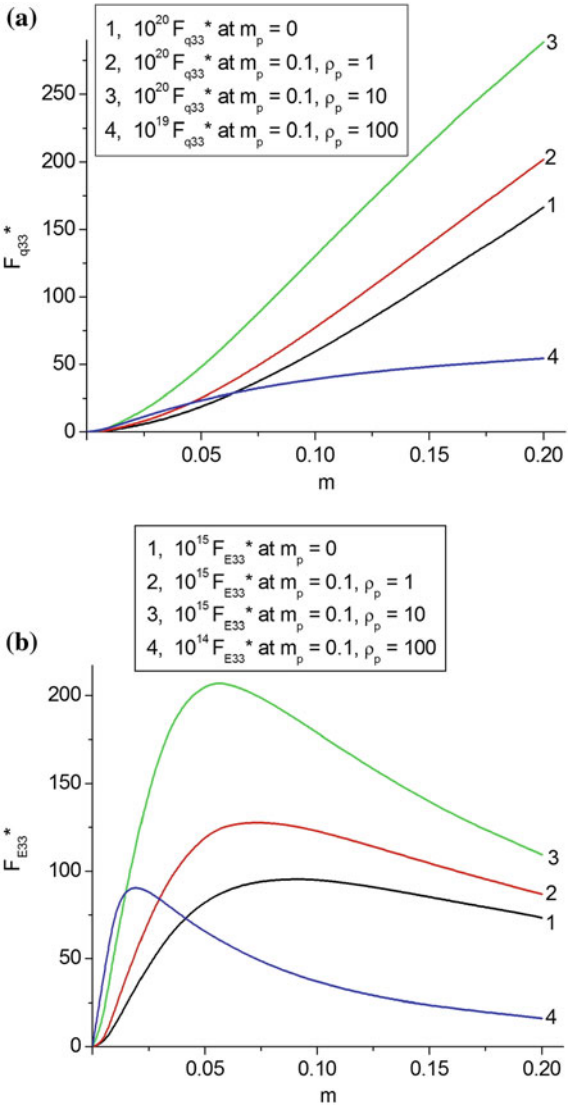

Fig. 3.14 Volume-fraction dependences of squared figures of merit $F^*_{q,33}$ (**a**) and $F^*_{E,33}$ (**b**) of the 1–3 PMN–0.33PT SC/polyurethane composite (at $m_p = 0$) and 1–3–0 PMN–0.33PT SC/porous polyurethane composite (at $m_p = 0.1$). The microgeometry of the 1–3–0 SC/porous polymer composite was described in Sect. 2.6.2

d^*_{3j}/s^{*E}_{jj} and the geometric size of the parallelepiped. The ratio of the coefficients of electromechanical transformation of the composite is represented as

$$r^*_N = \left(N^*_{33}/N^*_{31}\right) = \zeta^*_{d3j} s^{*E}_{33}/s^{*E}_{11}. \tag{3.18}$$

Equations (3.17) and (3.18) suggest that the anisotropy factor $\zeta_{d3j}{}^*$ and the ratio of elastic compliances concerned with longitudinal and transverse responses strongly influence r_{pow} and r_N.

Below we consider examples of the validity of inequalities

$$r^*_{pow} \geq 5 \tag{3.19}$$

and

$$\left|r^*_N\right| \geq 5 \tag{3.20}$$

which are caused by the piezoelectric and elastic anisotropy of the composite. Considerable variations of this anisotropy are observed, for instance, in the 1–3–0 FC/porous polymer composite (Fig. 2.10) with a regular arrangement of FC rods and air inclusions. It is assumed that the remanent polarisation of each FC rod is $\boldsymbol{P}_r^{(1)} \uparrow\uparrow OX_3$, and electrodes on the sample are parallel to the (X_1OX_2) plane (Fig. 2.10). To examine validity of conditions (3.19) and (3.20), we vary the following parameters of the composite: m, m_p and ρ_p.

In Table 3.16 we show volume-fraction (m) ranges that are related to the validity of conditions (3.19) and (3.20) in composites with different FC components and microgeometric characteristics of its porous matrix (m_p and ρ_p). As follows from Table 3.16, the volume-fraction ranges, wherein conditions (3.19) and (3.20) hold, become wider on the transition of a prolate shaped air inclusion in the polymer matrix (see inset in Fig. 2.10) to an oblate shape. This behaviour is a result of the important influence of elastic properties of the porous polymer matrix on composite properties. As follows from our analysis, as the aspect ratio of the air inclusion ρ_p increases at porosity m_p = const the ratios of elastic moduli $c^{(3)}_{33}/c^{(3)}_{13}$ and $c^{(3)}_{11}/c^{(3)}_{13}$ of the porous polymer significantly increase and lead to a more pronounced piezoelectric response of the composite along the OX_3 axis. The important role of the elastic properties of the matrix is additionally confirmed by data on the related 1–3 composites in the end part of Table 3.16. For the monolithic polyurethane matrix, the relation $c^{(3)}_{33}/c^{(3)}_{13} = c^{(3)}_{11}/c^{(3)}_{13} = 1.7$ is valid, and these ratios are approximately equal to the similar ratios related to the FC components considered in Table 3.16.

Following conventional formulae [11, 12] for the piezoelectric medium, we find that the factor from the coefficient of electromechanical transformation N^*_{33} is represented [55] as follows:

$$d^*_{33}/s^{*E}_{33} = \left(2e^*_{31}s^{*E}_{13} + e^*_{33}s^{*E}_{33}\right)/s^{*E}_{33} = 2e^*_{31}\left(s^{*E}_{13}/s^{*E}_{33}\right) + e^*_{33}. \tag{3.21}$$

Because of $\left|s^{*E}_{13}\right| < s^{*E}_{33}$ and the large anisotropy of the piezoelectric coefficients e^*_{3j} in the 1–3-type composite [7, 10], a contribution from $2e^*_{31}\left(s^{*E}_{13}/s^{*E}_{33}\right)$ in (3.21) is small. As a consequence, the equality

$$d^*_{33}/s^{*E}_{33} = e^*_{33} \tag{3.22}$$

holds with an accuracy to 5% in the whole m range [55]. It should be added that the piezoelectric coefficient e^*_{33} linking the piezoelectric polarisation of the composite

Table 3.16 Volume-fraction ranges [m_1; m_2] wherein conditions (3.19) and (3.20) in 1–3-type FC-based composites are valid

ρ_p	m_p	Range [m_1; m_2] of validity of condition (3.19)	Range [m_1; m_2] of validity of condition (3.20)
1–3–0 ZTS-19 FC/porous polyurethane composite			
0.1	0.1	[0.001; 0.011]	[0.032; 0.700]
	0.2	[0.001; 0.003]	[0.018; 0.700]
	0.3	–	[0.010; 0.700]
1	0.1	[0.001; 0.023]	[0.040; 0.700]
	0.2	[0.001; 0.022]	[0.031; 0.700]
	0.3	[0.001; 0.020]	[0.024; 0.700]
10	0.1	[0.001; 0.112]	[0.031; 0.700]
	0.2	[0.001; 0.152]	[0.022; 0.700]
	0.3	[0.001; 0.164]	[0.016; 0.700]
100	0.1	[0.001; 0.321]	[0.007; 0.700]
	0.2	[0.001; 0.325]	[0.004; 0.700]
	0.3	[0.001; 0.312]	[0.003; 0.700]
1–3–0 PZT-5H FC/porous polyurethane composite			
0.1	0.1	[0.001; 0.013]	[0.038; 0.700]
	0.2	[0.001; 0.004]	[0.021; 0.700]
	0.3	–	[0.011; 0.700]
1	0.1	[0.001; 0.029]	[0.049; 0.700]
	0.2	[0.001; 0.037]	[0.037; 0.700]
	0.3	[0.001; 0.024]	[0.028; 0.700]
10	0.1	[0.001; 0.129]	[0.037; 0.700]
	0.2	[0.001; 0.169]	[0.025; 0.700]
	0.3	[0.001; 0.184]	[0.019; 0.700]
100	0.1	[0.001; 0.336]	[0.008; 0.700]
	0.2	[0.001; 0.338]	[0.004; 0.700]
	0.3	[0.001; 0.323]	[0.003; 0.700]
1–3–0 PCR-7M FC/porous polyurethane composite			
0.1	0.1	[0.001; 0.013]	[0.037; 0.700]
	0.2	[0.001; 0.004]	[0.021; 0.700]
	0.3	–	[0.012; 0.700]
1	0.1	[0.001; 0.026]	[0.047; 0.700]
	0.2	[0.001; 0.025]	[0.036; 0.700]
	0.3	[0.001; 0.023]	[0.028; 0.700]
10	0.1	[0.001; 0.120]	[0.036; 0.700]
	0.2	[0.001; 0.157]	[0.025; 0.700]
	0.3	[0.001; 0.168]	[0.019; 0.700]
100	0.1	[0.001; 0.309]	[0.008; 0.700]
	0.2	[0.001; 0.312]	[0.005; 0.700]
	0.3	[0.001; 0.299]	[0.003; 0.700]

(continued)

Table 3.16 (continued)

ρ_p	m_p	Range $[m_1; m_2]$ of validity of condition (3.19)	Range $[m_1; m_2]$ of validity of condition (3.20)
1–3 ZTS-19 FC/polyurethane composite			
–	0	[0.001; 0.023]	[0.054; 0.700]
1–3 PZT-5H FC/polyurethane composite			
–	0	[0.001; 0.029]	[0.065; 0.700]
1–3 PCR-7M FC/polyurethane composite			
–	0	[0.001; 0.027]	[0.064; 0.700]

and the external strain along the poling axis OX_3 [7] shows a weak dependence on elastic properties of the matrix in the 1–3-type composite due to the dominating role of its stiff FC rods oriented along OX_3. This is also illustrated by curve 1 in Fig. 3.15. As for the d^*_{31}/s^{*E}_{11} factor, it undergoes changes with increasing porosity m_p (see curves 2–4 in Fig. 3.15) that can be accounted for by changes in the elastic anisotropy of the porous polymer matrix. Increasing m_p at ρ_p = const leads to a larger elastic anisotropy of the porous matrix and influences the transverse piezoelectric response of the 1–3–0 composite. It should be added that monotonic dependences of d^*_{3j}/s^{*E}_{jj} on the volume fraction m at m_p = const and ρ_p = const are predicted for the 1–3-type composites based on PZT-type FCs, and largest values of d^*_{3j}/s^{*E}_{jj} (j = 1 and 3) are achieved at m = 1, i.e., in the FC.

In contrast to d^*_{3j}/s^{*E}_{jj}, the volume-fraction (m) dependence of the ratio of the coefficients of electromechanical transformation r_N* from (3.18) is non-monotonic for the same 1–3-type composites at m_p = const and ρ_p = const. Data from Table 3.17 show that the elastic anisotropy of the porous matrix influences the ratio of the coefficients of electromechanical transformation r_N* of the 1–3–0 composite.

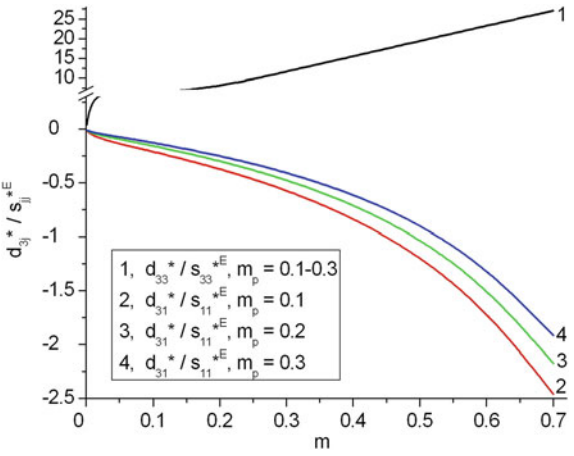

Fig. 3.15 Volume-fraction dependence of d^*_{3j}/s^{*E}_{jj} factors (in C/m^2, j = 1 and 3) related to the 1–3–0 PCR-7M FC/porous polyurethane composite at ρ_p = 100 (reprinted from paper by Topolov et al. [55], with permission from Taylor and Francis)

Table 3.17 Minimum values of r_N^* of the 1–3–0 PCR-7M FC/porous polyurethane composite at $m_p = 0.3$ and ratios that characterise the elastic anisotropy of the porous polyurethane matrix

ρ_p	$\min r_N^*$	$c_{33}^{(3)}/c_{13}^{(3)}$	$c_{11}^{(3)}/c_{13}^{(3)}$	$\left\|c_{33}^{(3)} - c_{11}^{(3)}\right\|/c_{13}^{(3)}$
0.1	–20.9 (at $m = 0.410$)	2.67	0.691	1.98
1	–17.3 (at $m = 0.405$)	1.70	1.08	0.62
10	–20.4 (at $m = 0.323$)	1.38	3.09	1.71
100	–31.7 (at $m = 0.157$)	1.36	29.9	28.5

The change in ρ_p of the porous matrix leads to changes in its elastic moduli $c_{ab}^{(3)}$. With increasing the $\left|c_{33}^{(3)} - c_{11}^{(3)}\right|/c_{13}^{(3)}$ ratio, values of $|\min r_N^*|$ increase (see the 2nd and 5th columns in Table 3.17). It is seen that $\min r_N^*$ is achieved at volume fractions of FC $0.157 \le m \le 0.410$, i.e., at the dominating volume fraction of porous polymer in the 1–3–0 composite. The revealed correlation (Table 3.17) also testifies to the important role of the elastic anisotropy of the porous polymer matrix in the formation of the piezoelectric performance and parameters (3.17), (3.18), (3.21), and (3.22) of the 1–3–0 composite in the wide volume-fraction (m) range.

The piezoelectric coefficients e_{3j}^* involved in (3.21) and (3.22) are of an independent interest for energy-harvesting applications. These piezoelectric coefficients are proportional to the coupling of electroded cantilevers [56] at one of the oscillations modes, either the '33' or '31' mode. In the 1–3-type composites based on FC or relaxor-ferroelectric SC, the inequality $e_{33}^* \gg \left|e_{31}^*\right|$ is valid within wide volume-fraction (m) ranges, and this condition favours an exploitation of a composite sample at the '33' mode. Since a minor max e_{33}^* appears at $0.9 < m < 1$, and e_{33}^* mainly increases with increasing m [7, 57], the FC (or SC) component becomes more suitable for piezoelectric energy harvesting in comparison to the related composite.

Data from Table 3.18 suggest that the piezoelectric coefficients e_{ij} of the perovskite-type FCs and domain-engineered relaxor-ferroelectric SCs vary in a relatively narrow range, i.e., typical values of $e_{ij} \sim$ (1–10) C/m^2. Positive values of e_{31} and a significant anisotropy of e_{3j} are important features of the $PbTiO_3$-type FCs with the large nisotropy of the piezoelectric coefficients d_{3j} [7, 41]. These characteristics of the $PbTiO_3$-type FCs strongly influence the piezoelectric properties of the related composites with connectivity patterns such as 1–3 [7, 40], 0–3 [7, 49], 2–2 [7], 1–1 [62], and 3–3 [63]. Finally, it should be noted that values of $|e_{3j}|$ of poled domain-engineered relaxor-ferroelectric SCs can be less than $|e_{3j}|$ of some FCs (see Table 3.18) despite the larger piezoelectric coefficients d_{3j} of these SCs. The reason for such a discrepancy is concerned with differences between elastic properties of the FCs and the SCs. It is obvious that these features of the piezoelectric materials are to be taken into account when selecting them for energy-harvesting applications.

Table 3.18 Experimental room-temperature values of piezoelectric coefficients e_{ij} (in C/m^2) of poled FCs and relaxor-ferroelectric SCs [7, 9, 10, 58–61][a]

	e_{31}	e_{33}	e_{15}
FCs[b]			
$BaTiO_3$ (I)	–4.4	18.6	11.6
$BaTiO_3$ (II)	–4.35	17.5	11.4
$(Ba_{0.917}Ca_{0.083})TiO_3$	–3.14	13.5	10.9
TBK-3	–3.2	12.5	9.1
TBKS	–0.68	7.71	4.56
NBS-1	–3.3	14.8	7.7
ZTS-19	–4.9	14.9	10.6
ZTS-24	–3.54	12.5	10.3
ZTSNV-1	–8.14	15.9	14.3
PZT-4	–5.2	15.1	12.7
PZT-5	–5.4	15.8	12.3
PZT-5H	–6.5	23.3	17.0
PZT-7A	–2.3	9.3	9.2
Navy Type VI	–6.5	23.3	17.0
PZ 27	–3.71	15.77	11.74
PZ 34	3.81	6.87	2.31
PCR-1, hp[c]	–3.7	11.1	10.8
PCR-7, hp	–9.0	28.3	17.9
PCR-7M, hp	–9.5	31.1	20.0
PCR-8, hp	–7.5	13.6	11.6
PCR-8, ct	–6.9	15.2	11.6
PCR-13, ct	–6.0	10.4	7.1
PCR-21, hp	–7.3	16.2	12.0
PCR-63, hp	–4.6	11.8	6.9
PCR-73, hp	–9.1	29.2	22.4
$Pb(Zr_{0.54}Ti_{0.46})O_3$	–1.86	9.0	9.8
$Pb(Zr_{0.52}Ti_{0.48})O_3$	–3.08	11.0	10.2
$(Pb_{0.94}Sr_{0.06})(Ti_{0.47}Zr_{0.53})O_3$	–5.2	15.1	12.7
Modified $PbTiO_3$ (I)	0.4	6.7	3.0
$(Pb_{0.9625}La_{0.025})(Ti_{0.99}Mn_{0.01})O_3$	1.32	6.80	3.35
$(Pb_{0.85}Nd_{0.10})(Ti_{0.99}Mn_{0.01})O_3$	1.80	8.83	5.41
$(Pb_{0.855}Nd_{0.11})(Ti_{0.94}Mn_{0.02}In_{0.04})O_3$	2.00	8.81	4.84
PMN– 0.35PT	–5.0	14.3	28.0
Domain-engineered [001]-poled SCs[d]			
PMN–0.30PT	–2.4	27.1	13.6
PMN–0.33PT	–3.9	20.3	10.1
PZN–0.08PT	–5.1	15.4	10.1

[a]See also references in the 1st column of Table 1.2

[b]∞mm symmetry

[c]FC samples of the PCR type have been manufactured using either the conventional technology (ct) or hot pressing (hp). PCR is the abbreviation for the group 'piezoelectric ceramics from Rostov-on-Don' (Russia) [7, 9]

[d]Macroscopic 4*mm* symmetry

It should be added that the shear oscillation mode can be of an independent interest for piezoelectric energy-harvesting applications. In work [64] a vibration energy harvesting device using the shear mode of the PMN–0.29PT SC has been designed and fabricated. In this device the high performance is achieved due to large values of the squared figure merit $d_{15}g_{15}$ concerned with the significant shear piezoelectric effect. According to experimental data [64], the studied domain-engineered SC is characterised by values of $d_{15}g_{15} = (261–267) \cdot 10^{-12}$ Pa^{-1}. These values are, for instance, by about 9 times larger than the squared figure of merit $(Q_{33})^2 = d_{33}g_{33} = 28.8 \cdot 10^{-12}$ Pa^{-1} related to the longitudinal piezoelectric effect in the domain-engineered PMN–0.28PT SC, a sample with the closest chemical composition (see data in Table 1.3). The $d_{15}g_{15}$ values are also by a few times larger than $(Q_{33})^2$ of the remaining PMN–xPT and PZN–yPT SCs listed in Table 1.3. It is believed that the shear oscillation mode and related effective parameters in piezo-active composites and their potential components will be a subject of studies in the future.

3.8 Conclusion

Chapter 3 has been devoted to the system of squared figures of merit that are concerned with the electromechanical properties of the piezoelectric medium and used to characterise its performance in the context of transducer, hydroacoustic and energy-harvesting applications. We have considered a number of examples of the squared figures of merit in conventional poled FCs and piezo-active composites based on either FCs or relaxor-ferroelectric SCs. The main results discussed in Chap. 3 are formulated as follows.

(i) The squared figures of merit have been analysed for poled FCs with the perovskite-type structure, piezo-active composites based on these FCs and piezo-active composites based on relaxor-ferroelectric SCs with a high piezoelectric activity. Among the connectivity patterns of interest for piezoelectric energy-harvesting and related applications, we mention 2–2, 1–3, 0–3, 1–0–3, and 1–3–0 systems.

(ii) The 2–2 PZT-type FC/polymer composite with a parallel connection of layers is of interest due to squared figures of merit $\left[Q^{*}_{3j}(m)\right]^2 \gg \left(Q^{(1)}_{3j}\right)^2$ (see Table 3.2), where the squared figures of merit $\left(Q^{(1)}_{3j}\right)^2$ (j = 1, 2 and 3) are related to FC.

(iii) The class of 2–2 parallel-connected composites based on PMN–0.28PT SCs with high piezoelectric activity and three variants of the poling direction of these SCs have been studied in detail. Examples of the polarisation orientation effects are related to the 2–2 composites with the SC components poled along one of the directions - [111], [001] or [011] in the perovskite

unit cell. The squared hydrostatic figure of merit $\left(Q_h^*\right)^2$ from (3.6) strongly depends on the rotation mode of the main crystallographic axes in the SC layer. For the 2–2 composite based on the [011]-poled PMN–0.28PT SC, the largest $\left(Q_h^*\right)^2$ value is achieved (Table 3.6) at the simplest orientation of the main crystallographic axes.

(iv) An additional opportunity to increase $\left(Q_h^*\right)^2$ is concerned with replacing the monolithic polymer component with an auxetic polymer. For instance, in the 2–2-type PIN-0.24-0.49 SC/auxetic polyethylene composite, the $\left(Q_h^*\right)^2$ value varies from about $150 \cdot 10^{-12}$ Pa^{-1} to $70 \cdot 10^{-12}$ Pa^{-1} at volume fractions of SC $m = 0.05$–0.10 (see Fig. 3.4).

(v) Condition (3.8) for the large anisotropy of the squared figures of merit $\left(Q_{3f}^*\right)^2$ in 2–2-type PMN–xPT/auxetic polyethylene composites is a result of the polarisation orientation effect, elastic anisotropy, and the relatively high piezoelectric activity of the SC component.

(vi) The 1–3-type PCR-7M FC/auxetic polyethylene composite is of interest due to large values of $\left(Q_{33}^*\right)^2$ (Table 3.8). For this composite system, a relatively large volume-fraction range is found wherein condition (3.8) $\left(Q_{3j}^*\right)^2$ holds. This is due to the active role of the auxetic component in forming the piezoelectric response of the composite.

(vii) The lead-free 1–3-type SC/auxetic polyethylene composites based on either KNN-TL or KNN-T SCs are advanced materials with high piezoelectric sensitivity [$g_{33}^* \sim (10^2$–$10^3)$ mV m/N], large squared figures of merit [$\left(Q_{33}^*\right)^2 \sim 10^{-11}$ Pa^{-1} and $\left(Q_h^*\right)^2 \sim (10^{-11}$ –$10^{-10})$ Pa^{-1}] (Fig. 3.9), and change in the sign of the piezoelectric coefficient d_{31}^*. This is due to the relatively high piezoelectric activity of the [001]-poled SC and elastic properties of the auxetic polymer component.

(viii) Examples of the 0–3-type composites based on the [001]-poled PMN – 0.33PT SC suggest that squared figures of merit $\left(Q_{3j}^*\right)^2$ and $\left(Q_h^*\right)^2$ strongly depend on the volume fraction of SC m and on the aspect ratio of SC inclusions ρ therein (see Table 3.9 and Fig. 3.10).

(ix) The new orientation effect in 1–0–3 composites with two contrasting ferroelectric components [i.e., highly piezo-active PMN–0.33PT SC (rods) and highly anisotropic $(Pb_{1-x}Ca_x)TiO_3$ FC (inclusions in a matrix, $x = 0.20$–0.25)] has been studied to show the high performance of these materials. We show the influence of the mutual orientation of the poling direction of SC and FC components on the properties of a 1–0–3 PMN–0.33PT SC/$(Pb_{1-x}Ca_x)TiO_3$ FC/araldite composite with $x = 0.20$–0.25. The elastic and piezoelectric anisotropy of the 0–3 FC/polymer matrix with prolate inclusions leads to values of $\left(Q_h^*\right)^2 \sim 10^{-11}$ Pa^{-1} in the aforementioned composite within specific volume-fraction and rotation-angle ranges due to a new orientation effect in the presence of a highly anisotropic 0–3 matrix.

The orientation effect leads also to a considerable anisotropy of squared figures of merit, and condition (3.8) holds within specific volume-fraction and rotation-angle ranges.

(x) The influence of the aspect ratio of FC inclusions ρ_i on the piezoelectric performance and hydrostatic parameters of the 1–0–3 composite based on [001]-poled PMN–0.33PT SC has been studied. A significant feature of this composite is that elastic properties of its 0–3 matrix strongly depend on ρ_i and influence the effective electromechanical properties of the 1–0–3 composite in wide aspect-ratio and volume-fraction ranges. Large values of the squared figures of merit $\left(Q_h^*\right)^2 \sim 10^{-11}\,\mathrm{Pa}^{-1}$ and $\left(Q_{33}^*\right)^2 \sim 10^{-10}\,\mathrm{Pa}^{-1}$ (Table 3.11 and Fig. 3.13b) and the validity of condition (3.13) make this composite attractive in hydrophone and piezoelectric energy-harvesting applications.

(xi) The important role of the elastic properties of the 0–3 FC/polymer matrix in forming the piezoelectric properties and figures of merit of the 1–0–3 PZN–0.08PT SC/modified $PbTiO_3$ FC/polyurethane composite has been discussed. Despite small negative values of the hydrostatic piezoelectric coefficients $d_h^{(1)}$ and $g_h^{(1)}$ of the SC component, this composite system is of interest due to large values of $\left(Q_{33}^*\right)^2$, $\left(Q_{31}^*\right)^2$ and $\left(Q_h^*\right)^2$ (Tables 3.13 and 3.14) which are achieved due to the pronounced piezoelectric anisotropy caused by the elastic properties of the 0–3 matrix with oblate FC inclusions. Moreover, condition (3.8) is valid for the 1–0–3 PZN–0.08PT SC/modified $PbTiO_3$ FC/polyurethane composite, i.e., in the presence of a polymer component with larger elastic compliances.

(xii) The system of figures of merit from (3.14) and (3.15) has been analysed for 1–3-type composites based on relaxor-ferroelectric SCs. The role of the porous polymer matrix in forming the piezoelectric response and anisotropy of squared figures of merit (see conditions 3.16) has been discussed. Large values of $\left(Q_{33}^*\right)^2$ and $F_{E,33}^*$ in comparison to those of the SC component (see Table 3.14 and Fig. 3.15) suggest that the 1–3–0 PMN–0.33PT SC/porous polyurethane composite at relatively small porosity (m_p = 0.1–0.2) in the polymer matrix can be effectively used in piezoelectric energy-harvesting applications.

(xiii) Effects of the porosity and microgeometry of the porous polymer matrix on the volume-fraction behaviour of the effective parameters and anisotropy factors in the 1–3-type composite have been analysed in the context of the elastic anisotropy of the matrix. Among the parameters to be of interest for energy-harvesting applications, we mention coefficients of electromechanical transformation and specific acoustic power [see (3.17) and (3.18)]. Their anisotropy considerably depends on the piezoelectric and elastic properties of the composite, and these properties can be varied due to changes in the microgeometry and porosity of the matrix. The correlation between the elastic anisotropy of the porous polymer matrix and minima of the ratio of specific acoustic powers N_{33}^*/N_{31}^* (Table 3.17) has been stated.

In general, knowledge of the figures of merit and related parameters as well as their dependences on microgeometry and content of the piezo-active composite is of benefit for design of novel high-effective piezoelectric energy-harvesting materials with preferable directions for the conversion and propagation of energy along specific directions.

References

1. Grekov AA, Kramarov SO, Kuprienko AA (1989) Effective properties of a transversely isotropic piezoelectric composite with cylindrical inclusions. Mech Compos Mater 25:54–61
2. Kim H, Tadesse Y, Priya S (2009) Piezoelectric energy harvesting. In: Priya S, Inman DJ (eds) Energy harvesting technologies. Springer, New York, pp 3–39
3. Uchino K, Ishii T (2010) Energy flow analysis in piezoelectric energy harvesting systems. Ferroelectrics 400:305–320
4. Priya S (2010) Criterion for material selection in design of bulk piezoelectric energy harvesters. IEEE Trans Ultrason Ferroelectr Freq Control 57:2610–2612
5. Bowen CR, Taylor J, Le Boulbar E, Zabeka D, Topolov VYu (2015) A modified figure of merit for pyroelectric energy harvesting. Mater Lett 138:243–246
6. Sessler GM, Hillenbrand J (2013) Figure of merit of piezoelectret transducers for pulse-echo or transmit-receive systems for airborne ultrasound. Appl Phys Lett 103:122904
7. Topolov VYu, Bowen CR (2009) Electromechanical properties in composites based on ferroelectrics. Springer, London
8. Safari A, Akdogan EK (eds) (2008) Piezoelectric and acoustic materials for transducer applications. Springer, New York
9. Dantsiger AYa, Razumovskaya ON, Reznitchenko LA, Grineva LD, Devlikanova RU, Dudkina SI, Gavrilyatchenko SV, Dergunova NV, Klevtsov AN (1994) Highly effective piezoceramic materials (Handbook). Kniga, Rostov-on-Don (in Russian)
10. Topolov VYu, Bisegna P, Bowen CR (2014) Piezo-active composites. Orientation effects and anisotropy factors. Springer, Heidelberg
11. Ikeda T (1990) Fundamentals of piezoelectricity. Oxford University Press, Oxford
12. Zheludev IS (1971) Physics of crystalline dielectrics, vol 2. Electrical properties. Plenum, New York
13. Gururaja TR, Safari A, Newnham RE, Cross LE (1988) Piezoelectric ceramic-polymer composites for transducer applications. In: Levinson M (ed) Electronic ceramics: properties, devices, and applications. Marcel Dekker, New York Basel, pp 92–128
14. Akdogan EK, Allahverdi M, Safari A (2005) Piezoelectric composites for sensor and actuator applications. IEEE Trans Ultrason Ferroelectr Freq Control 52:746–775
15. Safari A, Akdogan EK (2006) Rapid prototyping of novel piezoelectric composites. Ferroelectrics 331:153–179
16. Zhang R, Jiang B, Cao W (2001) Elastic, piezoelectric, and dielectric properties of multidomain $0.67Pb(Mg_{1/3}Nb_{2/3})O_3$–$0.33PbTiO_3$ single crystals. J Appl Phys 90:3471–3475
17. Fu H, Cohen RE (2000) Polarization rotation mechanism for ultrahigh electromechanical response in single-crystal piezoelectrics. Nature 403:281–283
18. Peng J, Luo H, He T, Xu H, Lin D (2005) Elastic, dielectric, and piezoelectric characterization of $0.70Pb(Mg_{1/3}Nb_{2/3})O_3$–$0.30PbTiO_3$ single crystal. Mater Lett 59:640–643
19. Wang F, He C, Tang Y (2007) Single crystal $0.7Pb(Mg_{1/3}Nb_{2/3})O_3$–$0.3PbTiO_3$/epoxy 1–3 piezoelectric composites prepared by the lamination technique. Mater Chem Phys 105:273–277
20. Ren K, Liu Y, Geng X, Hofmann HF, Zhang QM (2006) Single crystal PMN–PT/epoxy 1–3 composite for energy-harvesting application. IEEE Trans Ultrason Ferroelectr Freq Control 53:631–638

21. Topolov VYu, Krivoruchko AV (2009) Polarization orientation effect and combination of electromechanical properties in advanced $0.67Pb(Mg_{1/3}Nb_{2/3})O_3$–$0.33PbTiO_3$ single crystal/polymer composites with 2–2 connectivity. Smart Mater Struct 18:065011
22. Liu G, Jiang W, Zhu J, Cao W (2011) Electromechanical properties and anisotropy of single- and multi-domain $0.72Pb(Mg_{1/3}Nb_{2/3})O_3$–$0.28PbTiO_3$ single crystals. Appl Phys Lett 99:162901
23. Kar-Gupta R, Venkatesh TA (2008) Electromechanical response of piezoelectric composites: Effects of geometric connectivity and grain size. Acta Mater 56:3810–3823
24. Zhang R, Jiang B, Cao W (2003) Single-domain properties of $0.67Pb(Mg_{1/3}Nb_{2/3})O_3$–$0.33PbTiO_3$ single crystals under electric field bias. Appl Phys Lett 82:787–789
25. Cao HV, Schmidt H, Zhang R, Cao W, Luo H (2004) Elastic, piezoelectric, and dielectric properties of $0.58Pb(Mg_{1/3}Nb_{2/3})O_3$–$0.42PbTiO_3$ single crystal. J Appl Phys 96:549–554
26. Sessler G (1981) Piezoelectricity in polyvinylidenefluoride. J Acoust Soc Am 70:1596–1608
27. Topolov VYu, Bowen CR, Krivoruchko AV (2013) Role of domain orientations in forming the hydrostatic performance of novel 2–2 single crystal/polymer composites. Ferroelectrics 444:84–89
28. Grekov AA, Kramarov SO, Kuprienko AA (1987) Anomalous behavior of the two-phase lamellar piezoelectric texture. Ferroelectrics 76:43–48
29. Topolov VYu, Krivoruchko AV, Bowen CR (2012) Anisotropy of electromechanical properties and hydrostatic response of advanced 2–2-type composites. Phys Status Solidi A 209:1334–1342
30. Sun E, Cao W, Jiang W, Han P (2011) Complete set of material properties of single domain $0.24Pb(In_{1/2}Nb_{1/2})O_3$-$0.49Pb(Mg_{1/3}Nb_{2/3})O_3$-$0.27PbTiO_3$ single crystal and the orientation effects. Appl Phys Lett 99:032901
31. Groznov IN (1983) Dielectric permittivity. In: Physics encyclopaedia. Sovetskaya Entsiklopediya, Moscow, pp 178–179 (in Russian)
32. Bowen CR, Topolov VYu (2014) Polarisation orientation effects and hydrostatic parameters in novel 2–2 composites based on PMN-*x*PT single crystals. Ferroelectrics 466:21–28
33. Topolov VYu, Filippov SE, Bisegna P (2012) Anisotropy factors and hydrostatic parameters of 1–3-type piezo-active composites with auxetic polymer matrices. Ferroelectrics 432:92–102
34. Topolov VYu, Panich AE (2009) Problem of piezoelectric sensitivity of 1–3-type composites based on ferroelectric ceramics. Ferroelectrics 392:107–119
35. Topolov VYu, Turik AV (2001) Porous piezoelectric composites with extremely high reception parameters. Tech Phys 46:1093–1100
36. Dunn ML, Taya M (1993) Micromechanics predictions of the effective electroelastic moduli of piezoelectric composites. Int J Solids Struct 30:161–175
37. Dunn ML, Taya M (1993) An analysis of piezoelectric composite materials containing ellipsoidal inhomogeneities. Proc R Soc (Lond), Pt A 443:265–287
38. Dunn ML, Wienecke HA (1997) Inclusions and inhomogeneities in transversely isotropic piezoelectric solids. Int J Solids Struct 34:3571–3582
39. Huang JH, Yu S (1994) Electroelastic Eshelby tensors for an ellipsoidal piezoelectric inclusion. Compos Eng 4:1169–1182
40. Topolov VYu, Bisegna P, Krivoruchko AV (2008) Features of electromechanical properties of 1–3 composites based on $PbTiO_3$-type ceramics. J Phys D Appl Phys 41:035406
41. Glushanin SV, Topolov VYu, Krivoruchko AV (2006) Features of piezoelectric properties of 0–3 $PbTiO_3$-type ceramic/polymer composites. Mater Chem Phys 97:357–364
42. Bezus SV, Topolov VYu, Bowen CR (2006) High-performance 1–3-type composites based on $(1 - x)$ $Pb(A_{1/3}Nb_{2/3})O_3$–$xPbTiO_3$ single crystals (A = Mg, Zn). J Phys D Appl Phys 39:1919–1925
43. Topolov VYu, Krivoruchko AV, Bisegna P, Bowen CR (2008) Orientation effects in 1–3 composites based on $0.93Pb(Zn_{1/3}Nb_{2/3})O_3$–$0.07PbTiO_3$ single crystals. Ferroelectrics 376:140–152
44. Topolov VYu, Bowen CR, Bisegna P, Krivoruchko AV (2015) New orientation effect in piezo-active 1–3-type composites. Mater Chem Phys 151:187–195

45. Topolov VYu, Bowen CR, Bisegna P (2015) New aspect-ratio effect in three-component composites for piezoelectric sensor, hydrophone and energy-harvesting applications. Sens Actuators A—Phys 229:94–103
46. Topolov VYu, Bowen CR, Bisegna P, Panich AE (2015) Effect of the matrix subsystem on hydrostatic parameters of a novel 1–3-type piezo-composite. Funct Mater Lett 8:1550049
47. Topolov VYu, Bowen CR (2015) High-performance 1–3-type lead-free piezo-composites with auxetic polyethylene matrices. Mater Lett 142:265–268
48. Bisegna P (2015) Private communication
49. Topolov VYu, Bisegna P, Bowen CR (2011) Analysis of the piezoelectric performance of modern 0–3-type composites based on relaxor-ferroelectric single crystals. Ferroelectrics 413:176–191
50. Xu Y (1991) Ferroelectric Materials and their Applications. North-Holland, Amsterdam
51. Topolov VYu, Bowen CR, Filippov SE (2012) High performance of novel 1–3-type composites based on ferroelectric PZT-type ceramics. Ferroelectrics 430:92–97
52. Zhang S, Li F (2012) High performance ferroelectric relaxor-$PbTiO_3$ single crystals: Status and perspective. J Appl Phys 111:031301
53. Topolov VYu, Bowen CR, Isaeva AN (2016) Figures of merit and related parameters of modern piezo-active 1–3-type composites for energy-harvesting applications. In: Parinov IA, Chang S-H, Topolov VYu (eds) Proceedings of the 2015 International conference on Physics, mechanics of new materials and their applications. Nova, New York (in press)
54. Sverdlin GM (1990) Applied Hydroacoustics. Soodostroyeniye, Leningrad (in Russian)
55. Topolov VYu, Filippov SE, Panich AE, Panich EA (2014) Highly anisotropic 1–3–0 composites based on ferroelectric ceramics: microgeometry—volume-fraction relations. Ferroelectrics 460:123–137
56. Kim M, Kim S-H, Hong S (2013) Materials and devices for MEMS piezoelectric energy harvesting. In: Elvin N, Erturk A (eds) Advances in energy harvesting methods. Springer, New York, pp 417–435
57. Topolov VYu, Glushanin SV (2002) Evolution of connectivity patterns and links between interfaces and piezoelectric properties of two-component composites. J Phys D Appl Phys 35:2008–2014
58. Topolov VYu, Panich AE (2008) Electromechanical properties of poled ferroelectric ceramics based on peroskite-family oxides. Issledovano v Rossii, Reg. No. 002, pp 8–26 (in Russian). http://zhurnal.ape.relarn.ru/articles/2008/002.pdf
59. Khoroshun LP, Maslov BP, Leshchenko PV (1989) Prediction of effective properties of piezo-active composite materials. Naukova Dumka, Kiev (in Russian)
60. Luchaninov AG (2002) Piezoelectric effect in non-polar heterogeneous ferroelectric materials. Volgograd State Academy of Architecture and Construction, Volgograd (in Russian)
61. Nagatsuma K, Ito Y, Jyomura S, Takeuchi H, Ashida S (1985) Elastic properties of modified $PbTiO_3$ ceramics with zero temperature coefficients. In: Taylor GW (ed) Ferroelectricity and Related Phenomena, vol 4., PiezoelectricityGordon and Breach Science Publishers, New York, pp 167–176
62. Glushanin SV, Topolov VYu (2001) Features of electromechanical properties of piezoelectric composites with elements of connectivity 1–1. J Phys D Appl Phys 34:2518–2529
63. Bowen CR, Topolov VYu (2003) Piezoelectric sensitivity of $PbTiO_3$-based ceramic/polymer composites with 0–3 and 3–3 connectivity. Acta Mater 51:4965–4976
64. Ren B, Or SW, Wang F, Zhao X, Luo H, Li X, Zhang Q, Di W, Zhang Y (2010) Piezoelectric energy harvesting based on shear mode $0.71Pb(Mg_{1/3}Nb_{2/3})O_3$-$0.29PbTiO_3$ single crystals. IEEE Trans Ultrason Ferroelectr Freq Control 57:1419–1425